# Evaluation of ride comfort by data-driven virtual sensing of unsprung mass vertical velocity

RO57035: RO MSc Thesis

Pavan Prasad Hariharapura Guruprasad

Delft University of Technology


TU Delft

# Evaluation of ride comfort by data-driven virtual sensing of unsprung mass vertical velocity

by

Pavan Prasad Hariharapura Guruprasad

Student number: 5508053
Supervisor: Dr. Barys Shyrokau
Date submitted: Sunday 19th November, 2023

TU Delft

# Contents

# List of Figures

# List of Tables

# 1 Introduction

## 1.1. Project Background

According to statistics, there were 56.4 million sales of passenger cars around the world in 2021 alone. The automotive industry is experiencing increased levels of competition as a direct result of the increased demand for passenger vehicles. Because of this, customers have higher expectations regarding the performance of vehicles and the level of comfort they provide during rides.

The suspension system is an essential component of any vehicle and has a substantial impact on the vehicle's overall performance, handling, and safety. Here are a few of the most important reasons why the suspension system is so crucial:

- Ride comfort: The suspension system is responsible for absorbing road bumps and vibrations, providing passengers with a smoother and more comfortable ride. Not only is this important for passenger comfort, but also for reducing driver fatigue and enhancing vehicle handling.
- Stability: The suspension system aids in keeping the tyres in contact with the road, thereby improving traction, stability, and control. Maintaining vehicle stability during cornering, braking, and acceleration is crucial for preventing accidents and ensuring driver safety.
- Handling: The suspension system plays a crucial role in improving the vehicle's cornering ability, reducing body roll, and minimising weight transfer during acceleration and braking. This is essential for enhancing driver confidence and control, particularly in difficult driving conditions.
- Tire wear: The suspension system helps to evenly distribute the vehicle's weight across all four tires, thereby reducing tyre wear and extending tyre life. This is essential for reducing maintenance costs and maximising vehicle efficiency.
- Impact resistance: The suspension system is designed to absorb impacts and prevent collision-related damage to the vehicle and its occupants. This is essential for ensuring passenger safety and minimising injury risk in the event of an accident.

The design of the suspension is such that it allows for sufficient travel to accommodate both static and dynamic load variations. The relative displacement between the body and the various suspension parts is what we mean when we talk about suspension. In addition to this, the suspension needs to make sure that there is very little roll and pitch acceleration when the vehicle is being manoeuvred. Variations in the normal force exerted by the tyre can be used to characterize the wheel–road contact. There is a non-linear relationship between the maximum longitudinal and lateral tyre forces, also known as the maximum braking forces, and the normal force that is exerted by the tyre. As a result of this non-linear relationship, optimal handling performance can be accomplished with only slight variations in the normal force exerted by the tire. The transmission of road disturbances to the body of the vehicle is what's meant to be meant by the term "road isolation." Road isolation and, consequently, ride comfort are both improved when the transmissibility of the surface is reduced. Because maintaining contact with the road and minimizing road noise are mutually exclusive goals, the design of the suspension

system must incorporate a compromise between the two.

Dependent and independent suspension systems are the two categories that can be used to describe suspension setups. The dependent suspension system features a solid axle that runs the length of the frame and is supported by two separate springs. It makes it possible for the wheels on the left side as well as the right side to be connected to one another and to work together as a unit. Off-roading and applications that require high load handling are typical places to find vehicles equipped with this type of suspension. Leaf springs, Panhard rods, Watt's linkages, and other similar mechanisms are all examples of dependent suspensions.

Each wheel in an independent suspension system responds differently to the conditions of the road. This means that a bump on one side of the vehicle does not cause a reaction on the other side of the vehicle. When greater ride comfort and handling performance are required, these suspensions are the ones that are used. There are many different kinds of independent suspensions, such as the MacPherson strut, the multi-link suspension, the double wishbone suspension, and so on.

The three types of suspension systems—passive, semi-active, and active—are categorized according to the amount of control they provide over the vehicle's suspension. A mechanical spring and a passive damper are utilized in a passive suspension system, which ultimately results in the spring stiffness and damping characteristics remaining constant. By doing so, a satisfactory balance is achieved between the ride comfort and the handling of the vehicle. In practice, the passive suspension system performs the function of an open-loop control system. Only under certain conditions is it intended to perform at its highest level, which was the primary motivation behind its design. The passive suspension system is rigid and does not offer any degree of adjustability.

In semi-active systems, it is possible to exert control over one or more of the coefficients. In most cases, this is accomplished by utilizing a hydraulic damper system that is equipped with control valves that, depending on the suspension velocity, can adjust the damping coefficient of the suspension system. The passive system has already seen a significant improvement as a result of this, and it is now possible to tune it to obtain nearly optimal performance characteristics. The fact that the force generated by the actuator, which in most cases is a damper with variable force-velocity characteristics, is contingent on the direction in which the relative motion is taking place is the primary characteristic of semi-active systems[1]. This is considered a limitation because this suspension type cannot control the vehicle's ride height, roll, or pitch angle[2].

When a vehicle is equipped with an active suspension system, the suspension can be controlled by monitoring the state of the vehicle and applying an appropriate external force in order to achieve the highest possible level of driving performance. This system gathers data from a wide variety of required sensors, which results in an increase in both the system's power requirements and its overall cost. Between the unsprung mass and the sprung mass are some controllable actuators that have been installed. In this case, the force produced by the actuator does not depend in any way on the direction in which the relative motion is acting. This advantage controls the ride height in addition to compensating for the roll, pitch, and heave motions that the vehicle body experiences [2]. The suspension control module will individually adjust the damping forces for each wheel based on the information that it receives from the acceleration and suspension displacement sensors[3]. Figure 1.1 shows the damping capabilities of various suspension systems.

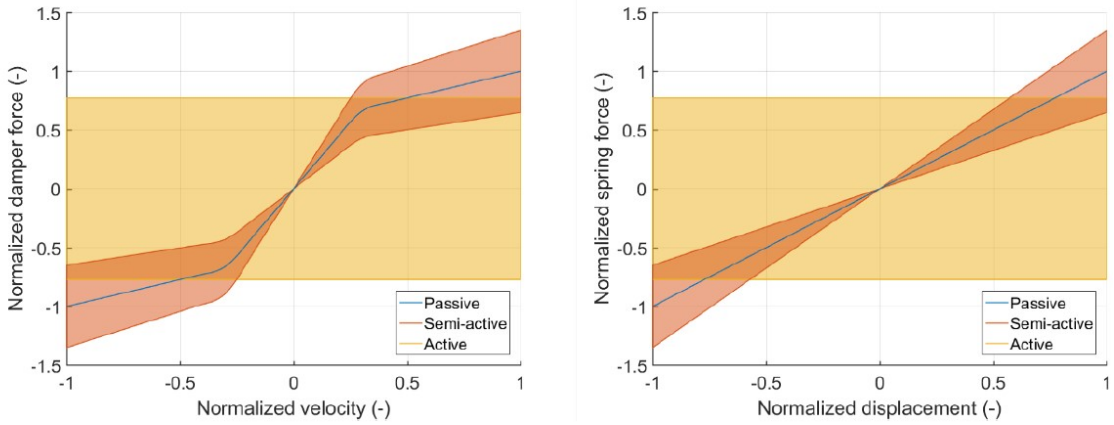


**Figure 1.1:** Force - velocity and force-displacement characteristics for passive, semi-active and active suspension systems. Coloured areas indicate the operation domain.

Despite the enhanced control capabilities offered by active suspension, it is accompanied by substantial energy consumption and remains expensive for widespread commercialization and implementation in economy class vehicles [4]. However, it is worth noting that certain suspension actuators have the capability to recover energy from road oscillations, thereby enhancing the overall energy efficiency of the system [5].

Controlled suspensions employ input data derived from acceleration sensors positioned on the suspension module as well as suspension displacement sensors located between the vehicle body and the lower control arms of the suspension system. In certain instances, supplementary acceleration sensors may also be positioned on the unsprung mass. Control systems often incorporate various additional inputs, including but not limited to steering wheel angle, vehicle speed, brake pressure, and other relevant factors.

The concept of ride comfort is commonly employed within the automotive sector to denote the subjective perception of passengers with regard to the level of smoothness and overall excellence of a vehicle's ride. The attainment of optimal ride comfort entails the reduction of the adverse effects caused by road irregularities and disturbances on the individuals within the vehicle, thereby facilitating an enjoyable and driving encounter.

Nevertheless, it should be noted that not all vibrations and motions experienced by the driver of a vehicle are directly perceptible. The driver's perception is limited to the motion and vibrations of the vehicle's body, specifically its sprung mass. When evaluating the perceived comfort of a vehicle, the primary aspect to consider is the vibrations caused by the sprung mass. This serves as a fundamental measure of vibrations, in order to assess comfort. The analysis of these accelerations will provide valuable insights into the behaviour of the sprung mass when subjected to various road inputs.

In active suspension, controllable actuators are installed between the unsprung and sprung masses. Further, acceleration sensors are placed on the sprung mass, and suspension displacement sensors are installed in the vehicle. Using these sensor data, the suspension control module individually adapts the damping forces for each wheel [3].

With the automotive industry increasingly advancing towards automated driving, sensors have become crucial components as they provide the data required to perceive the environment and vehicle state estimation [6]. However, incorporating sensors into suspension introduces complexity to the system and increases the vehicle's mass, production, and maintenance costs. Further, there are unmeasurable or complex quantities, which make sensing more difficult. With the increased number of parameters required to be measured, the virtual sensing of parameters becomes essential.

Virtual sensing takes signals from other physical sensors on board and combines them to get a

rough idea of the system's state and make virtual signals with values that have not been measured [7]. Even though virtual sensing implementation requires additional development costs, it will reduce repetitive maintenance intervals and costs [7]. Further, the possibility of diagnosing and predicting the system's state in advance also emerges [8]. Also, it helps in the interpretation of data and establishing unknown relationships between control variables. Virtual sensing is intensively used for automotive applications, for example, for passenger thermal comfort, the tire pressure monitoring system, powertrain applications, sprung mass state estimation, and others [9]. Virtual sensors can be classified into model-based and data-driven based on the method of sensor development.

In model-based virtual sensing, connections between inputs and outputs are described by mathematical equations, which make up a model [10]. Often, Kalman filters with vehicle models to update estimations are used [11]. The main advantages of model-based virtual sensing are predictability, explainability, and low experimental data requirements. A higher accuracy of prediction demands a more accurate model, which in turn demands a higher complexity model and higher computational capabilities. Hence, creating a model-based virtual sensor based on physical properties requires high competencies and skills. However, there are not many established unsprung mass velocity estimation models, and hence, developing a model-based virtual sensor will be hard.

Data-driven virtual sensing typically involves making use of machine learning techniques or statistical methods in order to analyse large amounts of data in order to extract patterns, relationships, or trends. This data can be gathered from sensors, simulations, experiments, or any number of other sources, and it can include a wide variety of types of data, including multivariate data, spatial data, or time series data. After that, the information is put to use in order to train a model of virtual sensing that has the ability to predict or estimate the behaviour of the system that is of interest.

One of the primary benefits of data-driven virtual sensing is that it can provide accurate predictions or estimates even when the underlying physical or virtual system is complicated, poorly understood, or difficult to measure directly. This is one of the most significant advantages of data-driven virtual sensing. It is also useful in circumstances in which the use of physical sensors would be prohibitively expensive or difficult to implement, or simply impossible due to concerns regarding public health or the environment. In addition, data-driven virtual sensing enables decision-making that is founded on real-time data and can be used for real-time monitoring, control, or optimisation of systems.

However, there are some restrictions associated with data-driven virtual sensing. Training the model requires a significant amount of data, and the accuracy and dependability of the virtual sensing model are susceptible to being affected by the quality and representativeness of the data that is used. The interpretability of the virtual sensing model may also be a challenge, as data-driven models may not provide explicit physical insights or explanations for their predictions. This could be a problem because data-driven models are becoming increasingly common. In addition, data-driven virtual sensing models are not appropriate for all kinds of systems. The availability and quality of data, in addition to the specific requirements of the system being modelled, all play a role in determining whether or not these models are applicable.

Viehweger et al. (2020) estimated tire forces using neural network-based virtual sensing [12]. Šabanovič et al. (2021) proved that NN-based VS could be used to estimate UM vertical velocity for a vehicle with passive suspension [13]. Further, Kojis et al. presented a technique to estimate unsprung mass vertical velocity in real-time using a neural network-based virtual sensor [14]. They presented a comparison between comfort metric RMS estimated for running with the same comfort algorithm (Skyhook algorithm) while using unsprung mass vertical velocities data from simulation and a virtual sensor.

Overall, data-driven virtual sensing is a powerful and flexible approach that leverages the power of data and machine learning to estimate or predict the behaviour of systems, even in the absence of explicit physical equations or measurements. This allows the approach to be used to estimate or predict the behaviour of systems in a variety of different contexts. It has a diverse range of applications across a variety of fields and is still a dynamic area of research and development.

## 1.2. Problem definition

The term ”unsprung mass velocity” refers to the vertical velocity of a vehicle’s parts not supported by the suspension system. These parts, which typically consist of the wheels, axles, and any other components that are directly connected to the suspension system, are subjected to vertical motion whenever the vehicle travels over bumps or obstacles, as well as over uneven road surfaces. The unsprung mass velocity is a crucial parameter in vehicle dynamics because of the direct influence it has on a vehicle’s ride comfort, its ability to handle corners, and its overall stability. Alterations in the velocity of the unsprung mass can have an effect on the contact between the road surface and the tyres, which in turn can have an effect on the tyre grip, traction, and the dynamic behaviour of the vehicle.

The ability to predict outcomes, the capability to explain results, and the low amount of data that is required are the primary benefits of model-based virtual sensing. However, a high level of model accuracy necessitates both a complex model and a high level of computational capability. Additionally, there are not many well-established models for estimating the unsprung mass velocity, which makes it difficult to create one.

This research aims to reduce the complexity of system to measure unsprung mass velocity through development of virtual sensor. Further, the impact of such a sensor on ride comfort, is to be evaluated which can be done by integrating the sensor with a suspension controller. Based on this background, the goal can be formulated as follows:

*” Evaluation of ride comfort by data-driven virtual sensing of unsprung mass vertical velocity.”*

The following sub-goals can be extracted from the goal:

- Development of a virtual sensor to estimate unsprung mass velocity using neural networks.
- Development of suspension controller using the virtual sensor for control of ride quality.
- Evaluation of the developed model for ride comfort performance.

## 1.3. Report outline

The report is structured as follows: Chapter 2 will explain the developed virtual sensor for unsprung mass velocity estimation and evaluates its performance.Chapter 3 will explain the suspension control methods and the proposed control approach. Chapter 4 evaluates the full vehicle performance with incorporation of the virtual sensor with the controller. Finally, chapter 5 will discuss the results shown in the previous chapters after which it is possible to draw final conclusions on this research, as well as allowing to suggest subjects for further research.

# 2

# Data-driven virtual sensor for unsprung mass velocity estimation

This chapter will provide a comprehensive analysis and explanation of the development and evaluation of a data-driven unsprung mass vertical velocity estimator. Further, it will assess the design choices and effect of related parameters on the developed model.

Data-driven virtual sensing of unsprung mass velocity means estimating or predicting the unsprung mass velocity by using data-driven models or algorithms. This method does not rely on taking direct measurements from physical sensors. This can be especially helpful when it is hard to use conventional physical sensors to measure the velocity of an unsprung mass, difficult to install, or sensors simply being unavailable. In this section, a neural network model is developed to estimate unsprung mass velocity using simulation-based dataset covering various scenarios. The developed virtual sensor was evaluated using a variety of different metrics that are considered to be industry standard. Further, the results are also plotted in time-series to have better understanding of the results from the model. In addition, the design decisions that were made for the creation of the model are analysed by looking into the effects of a number of different influencing parameters.

## 2.1. Dataset

The high-fidelity SUV model was used on the IPG CarMaker simulation platform, which was used to generate the dataset. IPG CarMaker is a software application that is developed specifically for the purpose of testing passenger cars and other light-duty vehicles. It makes use of a comprehensive vehicle model in addition to a multi-body system for the suspension of each individual wheel. It uses the TNO Delft Tyre, also known as the Magic Formula Swift tyre model for the tyre forces to generate realistic tyre forces. The parameters for mass-inertia, suspension kinematics, and compliance have been used to parameterize the model. Validation of the Delft-tire model was accomplished through testing on test benches. The vehicle model parameters used for the simulation is listed in Table 2.1.

| Parameter | Value |
|---|---|
| Vehicle overall mass (kg) | 1963.3 |
| Wheelbase (m) | 2.662 |
| CoG distance to front axle (m) | 1.093 |
| CoG distance to rear axle (m) | 1.569 |
| Front spring stiffness (N/m) | 25000 |
| Rear spring stiffness (N/m) | 30000 |
| Front damping (Ns/m) | 2500 |
| Rear damping (Ns/m) | 3000 |

**Table 2.1:** Simulation vehicle parameters

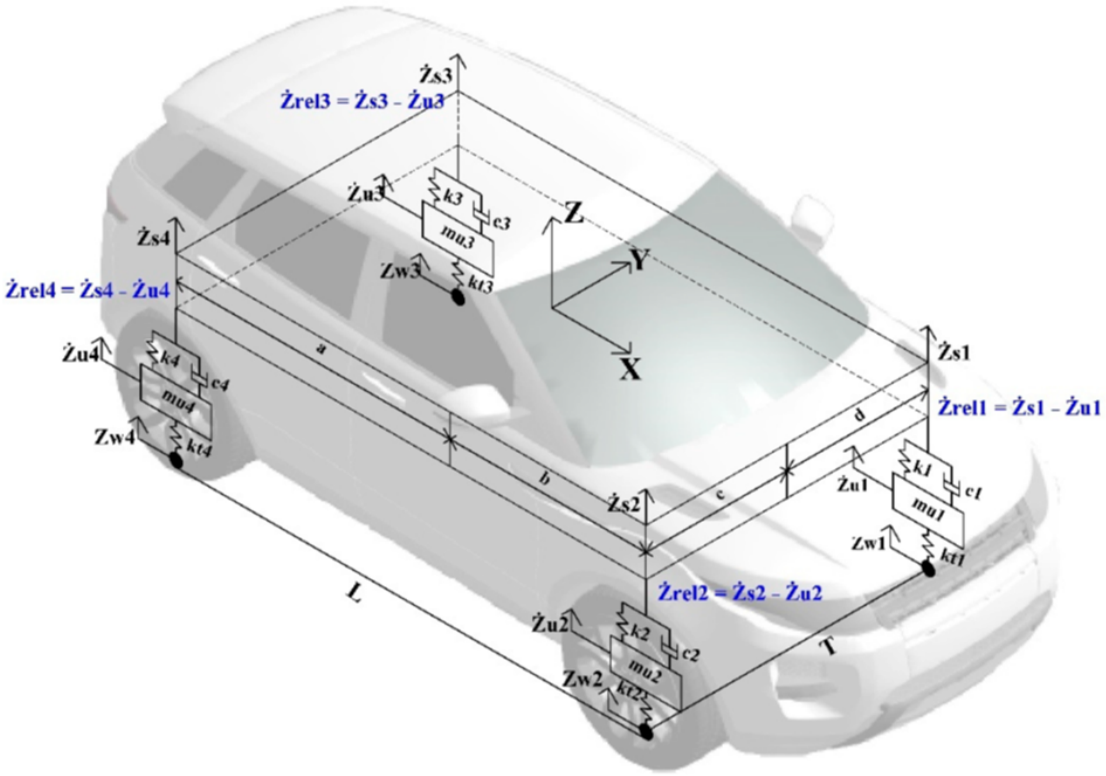


**Figure 2.1:** SUV dynamic model

The dataset includes the vehicle being driven at a variety of road profile parameters as well as at a range of driving speeds. Different profiles were selected so as to assess the acceleration levels. The first type of road that was used for simulations is the one that has parallel corrugations running the entire length of the test track. These ridges have a height of 25 millimetres and are evenly spaced with regard to the direction of the longitudinal axis. The height map of the digital road profile of the parallel corrugations are shown in Figure 2.2.

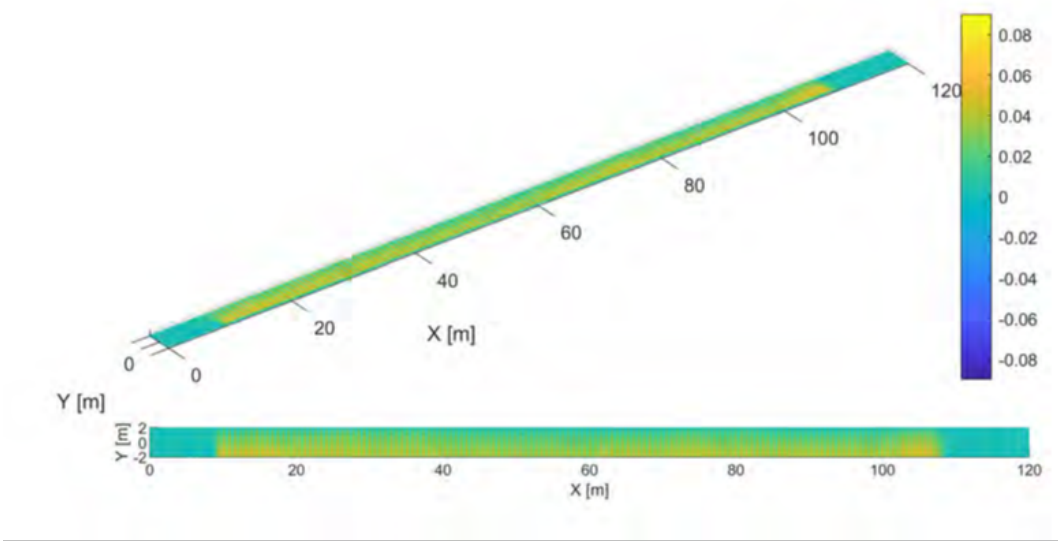


**Figure 2.2:** Height map of the 'Parallel corrugations' road used for full vehicle simulation

The angled corrugations road profile was the second one that was utilised. In this road profile, the corrugations are not entirely perpendicular to the longitudinal driving direction. Instead, the corrugations are angled by a varying angle along the length of the road in order to increase the amount of roll that is induced by the road displacements. The height map of the digital road profile of the angled corrugations are shown in Figure 2.3.

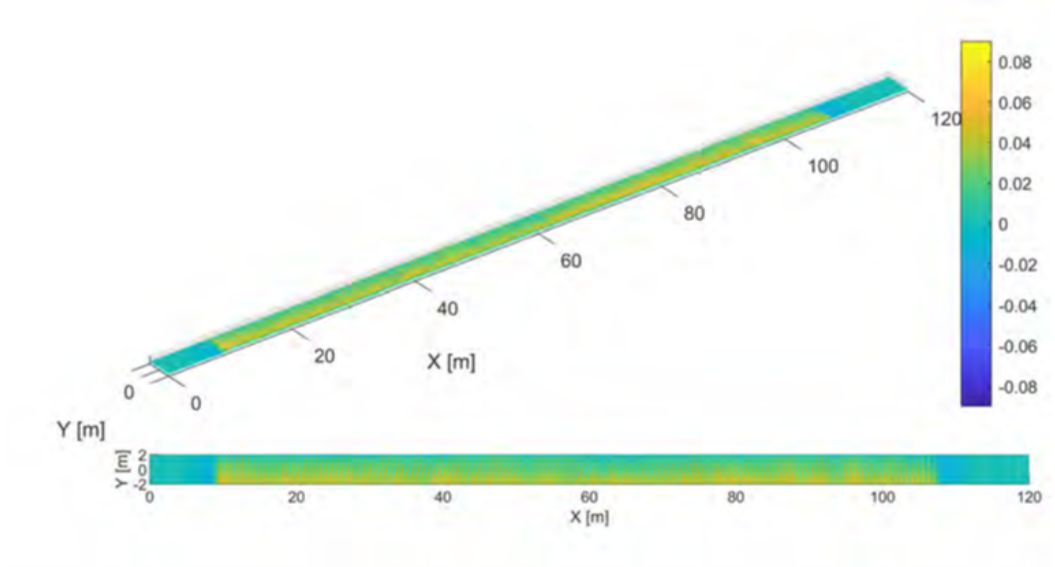


**Figure 2.3:** Height map of the 'Angled corrugations' road used for full vehicle simulation

The third road that is used for simulations is a road that is completely covered in cleats all the way along the test track. These cleats have the same amount of space between them along the longitudinal axis. The 'Fatigue' road is the final road profile that was used for the simulation. This road has been designed to accelerate the fatigue life of the suspension by performing repeatable and comparative suspension tests under simulated conditions. The continuous roughness of the road results in extreme vibrations in the vehicle. Fatigue road profiles are artificially created road surfaces that are designed to replicate the repetitive loading and unloading cycles experienced by vehicles on real roads. These repetitive loading and unloading cycles can cause passengers to become fatigued and uncomfortable. Engineers can study the effects of road roughness on ride comfort, performance, and durability of vehi-

cles and transportation systems when those systems are subjected to fatigue road profiles. This allows them to develop strategies to improve vehicle or system performance under conditions that are more representative of real-world driving. The height map of the digital road profile of the fatigue are shown in Figure 2.4.

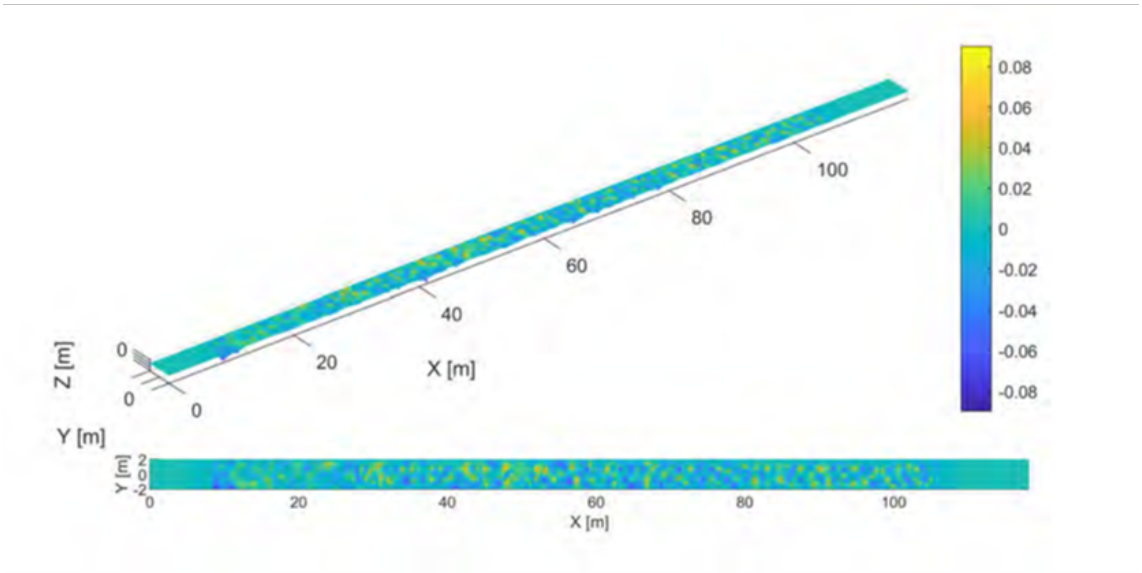


**Figure 2.4:** Height map of the 'Fatigue' road used for full vehicle simulation

Data was gathered on each of the road profiles at three distinct vehicle speeds: 10 km/h, 20 km/h, and 25 km/h. For the purpose of data collection, a sampling frequency of 100 Hz is utilised. The amount of time spent collecting data was restricted to a maximum of 30 seconds. Because of the restrictions imposed by the length of the road, the length of the dataset was cut to less than 30 seconds at higher speeds. In order to get rid of the flat road surface that would otherwise lead to the desired profile, the first ten seconds of each set of data are omitted. After that, the dataset is combined into a single matrix using a process called concatenation. After that, the dataset is shuffled around in a non-systematic manner, and it is then divided into three distinct sections: training, validation, and testing in the ratio of 0.6 to 0.2 to 0.2. The dataset that has been partitioned is then introduced into the network so that it can be used for their purposes in the appropriate manner.

| Test name | Vehicle speeds (km/h) | Time of data collection (s) |
|---|---|---|
| Parallel corrugations | 10 | 30 |
| | 20 | 24.48 |
| | 25 | 24.2 |
| Angled corrugations | 10 | 30 |
| | 20 | 30 |
| | 25 | 24.42 |
| Cleats | 10 | 30 |
| | 20 | 30 |
| | 25 | 29.62 |
| Fatigue road | 10 | 30 |
| | 20 | 21.15 |
| | 25 | 17.53 |

**Table 2.2:** Dataset description for the virtual sensor model development

There are a total of 12 parameters that serve as inputs for the dataset. These include the angle and rate of the driver's steering, the acceleration of the sprung mass in the z direction, the roll angle

and rate of the vehicle, the pitch angle and rate of the vehicle, and the angular velocity of each of the four wheels. Roll angle, also called roll angle of inclination or just roll, is the angle by which the body or chassis of a vehicle moves from its normal horizontal position. This angle is measured in degrees. Roll rate, on the other hand, is the speed or angle of rotation of a vehicle's body or chassis around its longitudinal axis, measured in degrees per unit of time. Pitch angle and pitch rate on the other hand refers to the angle and rate of rotation of vehicle body or chassis around its lateral axis. These parameters are are commonly measured in the industry. In order to facilitate the development of the model, it is assumed during the analysis phase that the roll and pitch parameters are easily accessible. The vertical velocities of the unsprung mass of all the four wheels were used as an output.

## 2.2. Neural-network model

A fully connected network, also called a dense layer or fully connected layer, is a type of layer in neural networks that is often used to process data with fixed input dimensions. It is the traditional type of layer used in many types of neural network architectures, such as feed-forward neural networks, multi-layer perceptrons (MLPs), and convolutional neural networks (CNNs).

In a fully connected layer, each neuron (or node) is connected to every other neuron in the layer above and the layer below it. This makes a graph with all connections. Each connection has a weight parameter, which is learned during training, and a bias term, which isn't always used. The output of a fully connected layer is calculated by taking a weighted sum of the inputs from the previous layer, running it through an activation function, and then sending the result to the next layer.

The fully connected layer is in charge of figuring out how the features in the input data are related to each other in complex, nonlinear ways. It changes the input data globally, which lets the network learn complex patterns and representations from the data. The number of neurons in the fully connected layer controls how many dimensions the output has, and the activation function makes the model nonlinear.

The model of a neural network for a virtual sensor that has been proposed can take in data in the form of a two-dimensional matrix, with the first dimension representing the sample and the second representing the number of signals. The matrix is fed into the fully connected network that was designed for that purpose. The summary of the proposed network is shown in Figure 2.5. The unsprung mass velocities of individual corner modules can be predicted with the help of four different networks like this one: FL, FR, RL and RR. Various network models with fewer layers were first tried in order to obtain the required estimation performance. The suggested network, however, was the most ideal and straightforward for the necessary estimating purpose.

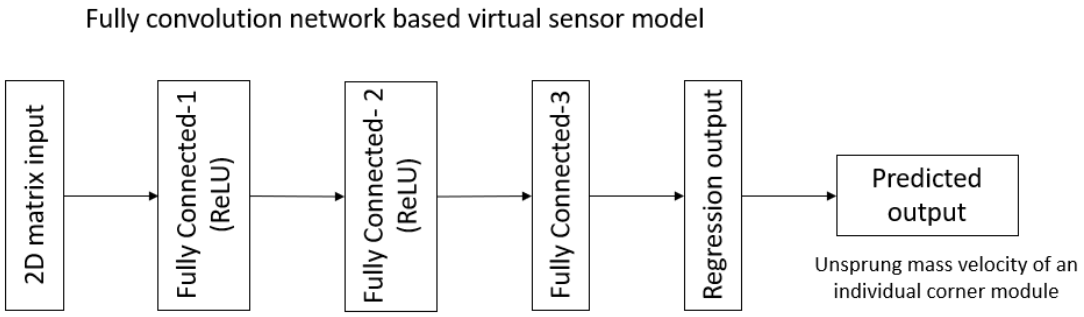


**Figure 2.5:** Structure of the neural-network based virtual sensor

| Name | Type | Number of neurons |
|---|---|---|
| input layer<br>12 features with 'zscore' normalization | Feature input | 12 |
| fc1<br>fully connected layer with 256 neurons | Fully connected | 256 |
| relu1<br>ReLU layer | ReLU | 256 |
| fc2<br>fully connected layer with 128 neurons | Fully connected | 128 |
| relu2<br>ReLU layer | ReLU | 128 |
| fc3<br>fully connected layer with 1 neuron | Fully connected | 1 |
| output layer<br>regression output with mean squared error optimization | Regression output | 1 |

**Table 2.3:** Summary of the proposed network

The input layer of the neural network has 12 input features, and z-score normalisation is applied to the input data. The job of the input layer is to turn the raw data into a format that the next layers of the network can understand and use. Z-score normalization, which is also known as standardization, is a technique that is commonly used in the preprocessing of data. Its purpose is to scale the features of a dataset so that they have a mean value of zero and a variance of one. This, in turn, helps to eliminate scale differences, reduces sensitivity to outliers, and supports convergence in optimisation.

The input layer is followed by a fully connected layer of the neural network containing 512 output neurons. Rectified linear unit (ReLU) layer of the neural network is used as an activation function. Rectified Linear Unit is an activation function that is often used in neural networks. It is a simple, piecewise linear function that adds non-linearity to the model and lets neural networks learn complex nonlinear relationships in the data.

The ReLU activation function is described in math as follows:

$$f(x) = max(0, x) \tag{2.1}$$

where x is what the function is given and f(x) is the output. In other words, ReLU gives back the input value if it is positive (greater than zero) and zero if it is negative (less than zero).

The second fully connected layer contains 256 output neurons. This layer also uses ReLU as activation function. The third fully connected layer contains 128 output neurons which again uses ReLU as activation function. The fourth fully connected layer of the neural network has 1 output neuron. The results of this network is fed into a regression output layer that performs regression (i.e., prediction of continuous values). Because of this, the network generates real-valued outputs, which are an estimation of probably output signals. The output is a vector consisting of an estimated value of the relative vertical velocity of the unsprung mass for one of the four suspension quarters (FL, FR, RL, and RR). This was done because the network performed better when used individually in comparison to when it was used as part of a single network that estimated all four parameters

The optimisation algorithm revises the model weights in accordance with the rate of learning. A higher initial learning rate could potentially accelerate initial convergence, but it would also cause the optimisation algorithm to overshoot the optimal weights. Convergence may be slowed down by lower initial learning rates, but the resulting weights will be more accurate over time. The results of performance evaluations carried out using a variety of learning rates led to the selection of an initial learning rate of 0.002. In addition, the learning rate scheduling strategy was utilised while the training was being conducted. This suggests that the learning rate will be updated at particular epochs in accordance with the rules that have been predefined. In order to achieve the best possible performance, the learning rate was reduced by a factor of 0.5 every 25 epochs. During the training session, this was done to

achieve better convergence while also minimising overshooting and oscillation.

Over-fitting is a phenomenon that occurs when a model learns to perform well on the training data but does not generalise well to data that it has not seen before. Regularisation is a technique that is used in machine learning and statistical modelling to prevent overfitting. During the training process, regularisation techniques add additional constraints or penalties to the model in order to prevent it from becoming overly complex and from fitting the training data to a greater extent than it should. The objective function of the model is penalised by L2 regularisation in the amount that is proportional to the squared values of the model's weights. This results in models having smaller weights all around, which effectively reduces the impact of individual weights and also reduces the model's sensitivity to small changes in the input data. The L2 regularisation was set to have a strength of 1E-7 based on various trails performed for network optimization.

In a neural network, the number of epochs is how many times the entire training dataset is run through the network during the training process. Each epoch has a forward pass, a backward pass, and possibly an evaluation step, where the model's performance is measured on a validation or test dataset. The number of epochs in a neural network depends on a number of things, such as how hard the problem is, how big the dataset is, how the model is built, and what optimisation algorithm is being used. The maximum number of epochs was set to 100.

## 2.3. Results and analysis

In this section, accuracy of developed virtual sensor is presented. First the performance metrics used for evaluation is discussed after which the results of the model is presented. Further, the effect of various parameters are evaluated in order to support the design choices.

### 2.3.1. Performance metrics

It is essential to select suitable evaluation metrics according to the particular problem at hand and the goals of the neural network model, and it is equally essential to interpret the results within the context of the problem domain. Both of these steps must be carried out in a timely manner.There are a few different performance evaluation metrics that are commonly used for regression models. These metrics provide insights into the generalisation ability and accuracy of the models.

#### Root mean squared error(RMSE)

The root mean squared error, or RMSE is the square root of the average of the squared differences between the predicted and actual values. It gives the average error value in the same units as the target variable. It is a common way to measure how well regression neural network models work, with lower values showing better performance. The maximum RMSE value indicates the greatest deviation between actual and predicted values in the data set. This value is significant because it indicates the model's maximum allowable error. The minimum RMSE value indicates the smallest deviation between actual and predicted values in the data set. This value is significant because it indicates the smallest error the model is capable of making.

$$RMSE = \sqrt{\frac{1}{n}\sum_{i=1}^{n}(v_{acti} - v_{viri})^2} \tag{2.2}$$

where,

- $v_{acti}$ = Unsprung mass velocity in vertical direction of the ith sample, [m/s]
- $v_{viri}$ = Unsprung mass velocity in vertical direction estimated by the virtual sensor of the ith sample, [m/s]

R-squared ($R^2$)
R squared, also known as the coefficient of determination, is a statistical measure that can be utilised to evaluate how well a regression model fits the data. It shows what percentage of the variation in the dependent variable can be attributed to the independent variable (or variables) in the regression model. It ranges from 0 to 1, with higher values indicating better model performance. A value of 1 indicates that the model explains all the variation in the target variable, while a value of 0 indicates that the model explains none of the variation.

$$R^2 = 1 - \frac{\sum_{i=1}^{n}(v_{acti} - v_{viri})^2}{\sum_{i=1}^{n}(v_{acti} - \bar{v_{act}})^2} \tag{2.3}$$

where,

- $v_{acti}$ = Unsprung mass velocity in vertical direction of the ith sample, [m/s]
- $v_{viri}$ = Unsprung mass velocity in vertical direction estimated by the virtual sensor of the ith sample, [m/s]
- $\bar{v_{act}}$ = Mean value of unsprung mass velocity in vertical direction, [m/s]

Mean absolute error(MAE)
The mean absolute error (MAE) is a statistical metric that measures the average absolute difference between predicted values and actual values in a set of data points. In other words, it compares the actual values to the predicted values. It is frequently applied in the context of evaluating the precision or effectiveness of a predictive model. Without taking into consideration which way the errors are going, the mean absolute error (MAE) is a measure of the typical magnitude of the errors produced by a model, with lower values showing better performance.

$$\text{Mean Absolute Error} = \frac{1}{n}\sum_{i=1}^{n}|v_{acti} - v_{viri}| \tag{2.4}$$

where,

- $v_{acti}$ = Unsprung mass velocity in vertical direction of the ith sample, [m/s]
- $v_{viri}$ = Unsprung mass velocity in vertical direction estimated by the virtual sensor of the ith sample, [m/s]

### 2.3.2. Results

The validation root mean squared error (RMSE), the testing RMSE, the $R^2$ value, and the mean absolute error are the key performance indicators that are utilised when evaluating the developed model. These values are determined for every wheel individually. The RMSE values for the testing dataset can be found in the Table 2.4. Both the root mean square error and the mean absolute error have the same units as the velocity that was measured. When it comes to predicting unsprung mass velocity, the newly developed virtual sensor has an error rate of 0.08 m/s on average. The R-squared value and the mean absolute error values are both quite satisfactory.

| **Unsprung mass velocity** | **Front left** | **Front right** | **Rear left** | **Rear right** |
|---|---|---|---|---|
| **Validation RMSE(m/s)** | 0.093 | 0.083 | 0.067 | 0.07 |
| **Testing RMSE(m/s)** | 0.087 | 0.081 | 0.068 | 0.067 |
| **$R^2$** | 0.957 | 0.97 | 0.978 | 0.982 |
| **Mean Absolute Error(m/s)** | 0.062 | 0.056 | 0.047 | 0.047 |

**Table 2.4:** Results of virtual sensor

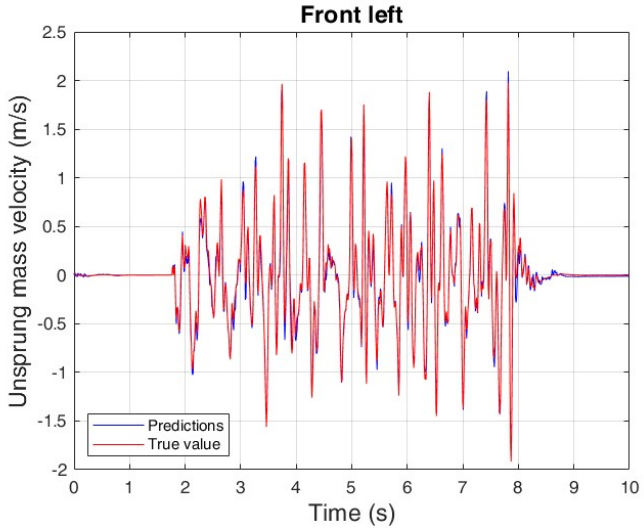


**(a)** Front left

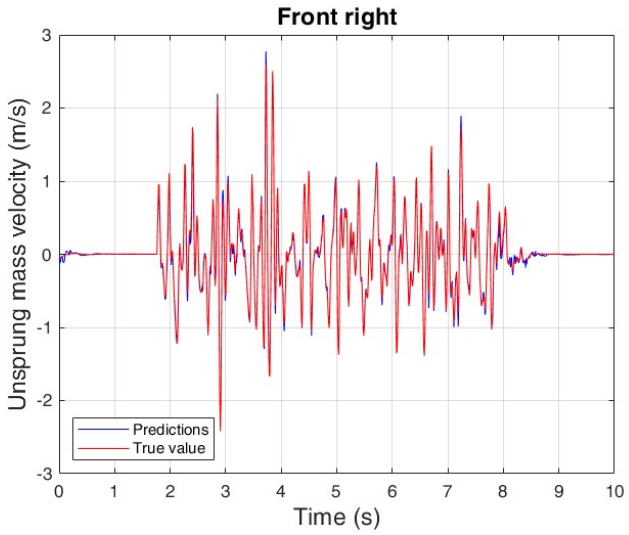


**(b)** Front right

**Figure 2.6:** Virtual sensor performance for the front wheels

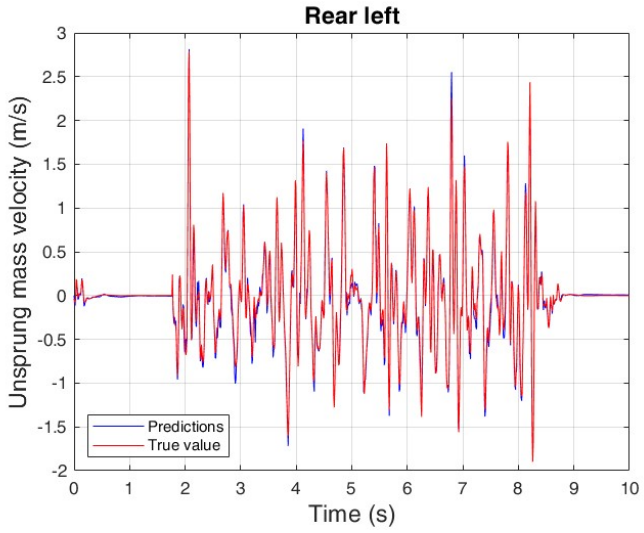


**(a)** Rear left

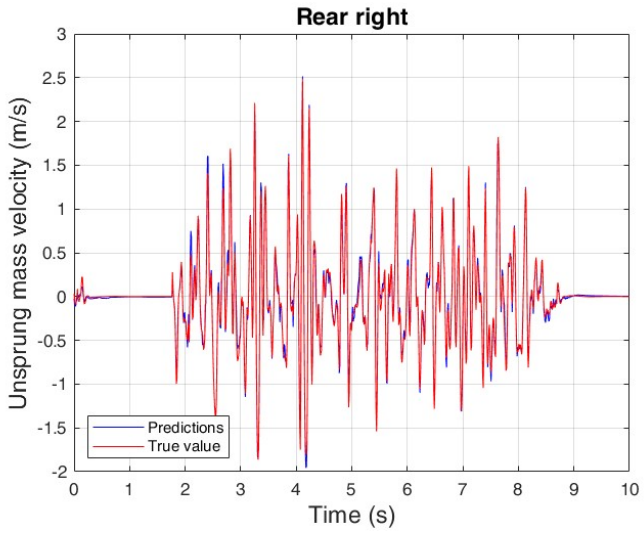


**(b)** Rear right

**Figure 2.7:** Virtual sensor performance for the rear wheels

The time-series virtual sensor performance for unsprung mass velocity estimations are plotted in Figure 2.6 and Figure 2.7. The plots demonstrate that the newly developed sensor estimates the parameter with a degree of accuracy that is quite comparable to that of the true values of estimation. Because the curves of actual data and those predicted by virtual sensor are so similar to one another, the accumulated numerical results from the virtual sensor are considered to be satisfactory.

### 2.3.3. Effect of parameters

In this section, the design choices are evaluated by investigating the effects of various parameters on the virtual sensor performance. The various parameters that are investigated are wheel steer angles against driver steering input, yaw against pitch and roll and the effect of acceleration values in other axes.

#### Wheel steer angles vs driver steering inputs

It is typically simpler to measure the steering inputs made by the driver than it is to measure the angles at which the wheels are turned. This is due to the fact that the driver's steering input can be easily measured with a steering wheel position sensor, which detects the angle and direction of the steering wheel as it is turned by the driver. This allows for the driver's steering input to be accurately measured. On the other hand, determining the angles of the wheels' steer requires a significantly more involved method. For this reason, it is customarily necessary to make use of sensors, such as wheel speed sensors, which can determine the speed and the direction in which the wheels are turning as they rotate. The signals from these sensors must then be processed to calculate the steer angle for each wheel. This makes driver steering inputs much more suitable for considering it as an input for the model as it is easier to measure.

The performance of the virtual sensor is evaluated taking into account the individual wheel steer angles, and then taking into account the driver's steering wheel angle and rate. In the first trial, the model is tested with the wheel steer angles as an input. In the subsequent trials, the model is tested by substituting the steering wheel angle and velocity for the steer angles. The performance of the virtual sensor is reported in Figure 2.8 and Table 2.5.

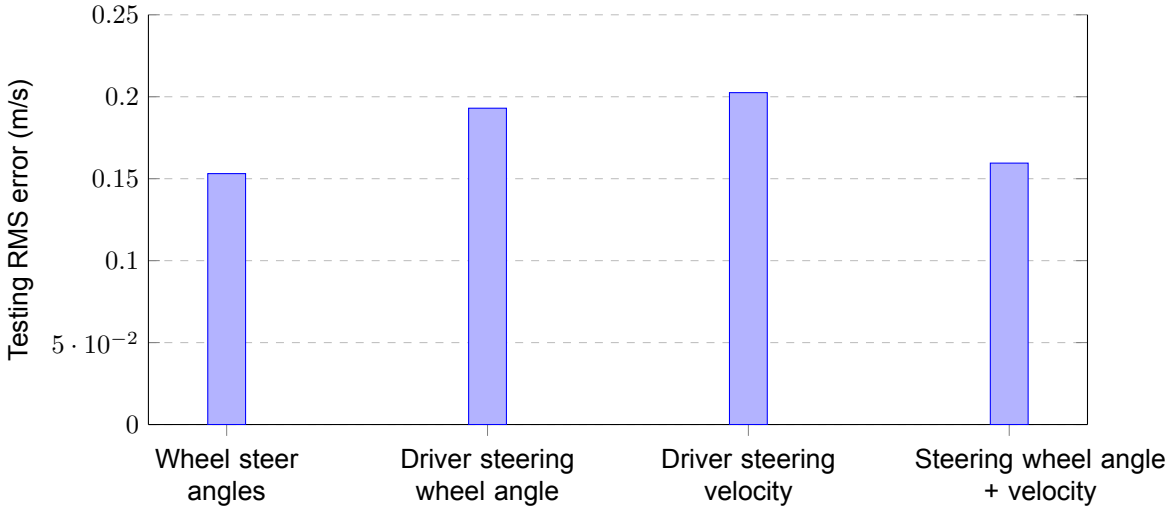


**Figure 2.8:** Effect of Wheel steer angle and driver steering inputs for training the model on unsprung mass vertical velocity.

| Unsprung mass velocity FL | RMSE | | $R^2$ | MAE |
|---|---|---|---|---|
| | Validation | Testing | | |
| **Wheel steer angles** | 0.1656 | 0.1531 | 0.8649 | 0.1024 |
| **Driver steering wheel angle** | 0.1960 | 0.1930 | 0.7900 | 0.1294 |
| **Driver steering velocity** | 0.2017 | 0.2025 | 0.7517 | 0.1395 |
| **Steering wheel angle + velocity** | 0.1610 | 0.1595 | 0.8512 | 0.1013 |

**Table 2.5:** Virtual sensor performance of wheel steer angle against driver steering inputs

The model performance deteriorates with replacing the wheel steer angles with steering wheel angle. This trend is also seen with steering wheel velocity as well. However, the model performance is

more or less similar when a combination of steering wheel angle and velocity is used. This makes the combination of driver steering inputs a more appropriate choice for modelling inputs, as it is easier to measure and has performance comparable to that of wheel steer angles.

### Yaw, pitch and roll

In three-dimensional space, yaw, pitch, and roll are terms used to describe the orientation of an object. Yaw is the rotation around the vertical axis, whereas pitch and roll refer to rotations around the lateral and longitudinal axes, respectively. The three angles are interdependent, meaning that a change in one angle will affect the other two. Depending on the application, different sensors can be used to measure yaw, pitch, and roll angles. Using an inertial measurement unit (IMU) consisting of three accelerometers and three gyroscopes is a common method. The accelerometers measure the acceleration in each direction, whereas the gyroscopes measure the rate of rotation about each axis.

The performance of the virtual sensor is evaluated taking into account the pitch, roll and yaw angles and rates individually and then taking into account the combinations between them. The performance of the virtual sensor is reported in Figure 2.9 and Table 2.6.

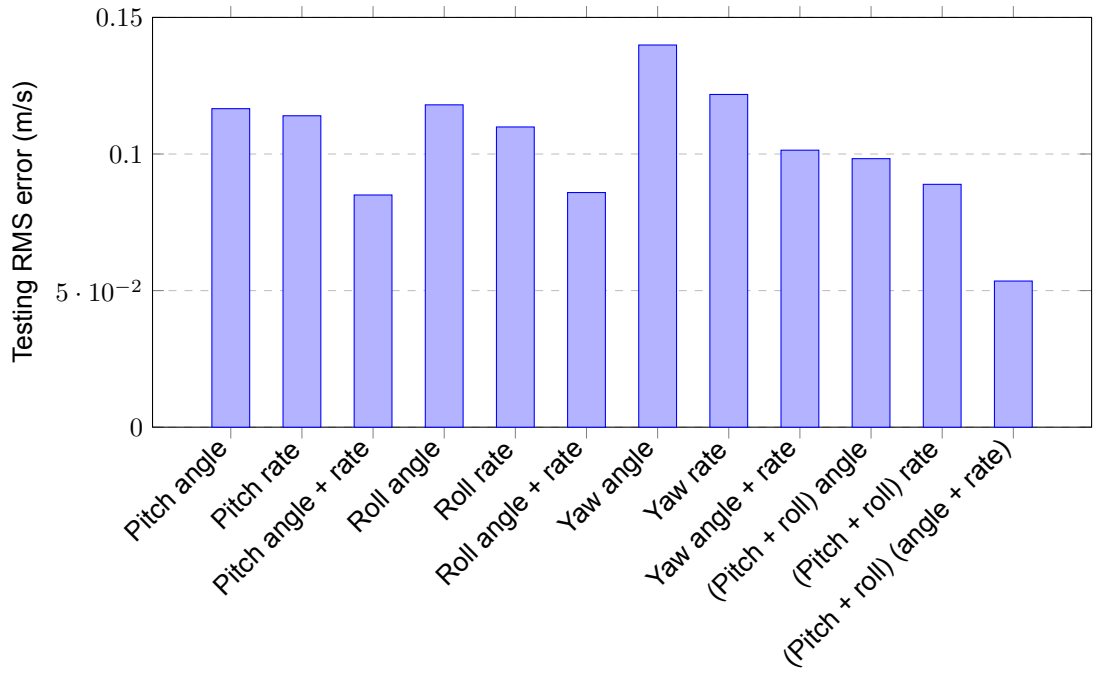


**Figure 2.9:** Effect of yaw, pitch and roll on testing RMS error.

| Unsprung mass velocity front left | RMSE(m/s) | | $R^2$ | Mean absolute error |
|---|---|---|---|---|
| | Validation | Testing | | |
| **Pitch angle** | 0.1140 | 0.1166 | 0.9207 | 0.0757 |
| **Pitch rate** | 0.1154 | 0.1140 | 0.9258 | 0.0761 |
| **Pitch angle + rate** | 0.0840 | 0.0850 | 0.9550 | 0.0565 |
| **Roll angle** | 0.1200 | 0.1180 | 0.9200 | 0.0800 |
| **Roll rate** | 0.1170 | 0.1099 | 0.9229 | 0.0716 |
| **Roll angle + rate** | 0.0800 | 0.0859 | 0.9595 | 0.0577 |
| **Yaw angle** | 0.1361 | 0.1399 | 0.8851 | 0.0942 |
| **Yaw rate** | 0.1199 | 0.1218 | 0.9100 | 0.0810 |
| **Yaw angle + rate** | 0.1035 | 0.1014 | 0.9405 | 0.0681 |
| **(Pitch + roll) angle** | 0.0970 | 0.0983 | 0.9480 | 0.0663 |
| **(Pitch + roll) rate** | 0.0780 | 0.0889 | 0.9533 | 0.0648 |
| **(Pitch + roll) angle + rate** | 0.05 | 0.0535 | 0.9844 | 0.036 |

**Table 2.6:** Virtual sensor performance: Effect of pitch, roll and yaw

When the pitch and roll angles, as well as their rates, are taken into consideration, the performance of the model is significantly better than before. Pitch and roll, in comparison to yaw, appear to have a greater influence on performance when the various scenarios and speeds are taken into consideration. However, their effects might have to be re-investigated when considering different scenarios and velocities of the vehicle.

### Sprung mass acceleration values in X and Y directions

The term ”sprung mass acceleration” refers to the acceleration of the portion of a vehicle supported by the suspension system (”sprung” mass) relative to the ground. When a vehicle is in motion, it encounters various forces that accelerate its components. The forces acting on the sprung mass include the force of the engine propelling the vehicle forward, as well as forces generated by braking, turning, and road imperfections. These forces accelerate the sprung mass in different directions. Longitudinal sprung mass acceleration(X) refers to the acceleration of the vehicle along the direction of travel. This acceleration is important because it influences the vehicle's acceleration and braking performance. Lateral sprung mass acceleration refers to the vehicle's acceleration perpendicular to its direction of travel. This acceleration is significant because it influences the handling and stability of the vehicle during cornering. Vertical sprung mass acceleration is the acceleration of a vehicle along its vertical axis. This acceleration is significant as it influences the ride comfort and suspension system performance of the vehicle.

The effect of these factors depends on the vehicle's speed, the defined manoeuvre, and numerous other variables. To determine their significance, the developed model is evaluated by comparing its performance when trained with acceleration values along all axes to its performance when trained with acceleration values along only the Z-axis. A sinusoidal manoeuvre of 15 deg amplitude and 0.5 Hz frequency is defined to intensify the effect of X and Y axes. Data was gathered on one of the road profiles (parallel corrugations) at three distinct vehicle speeds: 10 km/h, 20 km/h, and 25 km/h. For the purpose of data collection, a sampling frequency of 100 Hz is utilised. The amount of time spent collecting data was restricted to a maximum of 30 seconds. Because of the restrictions imposed by the length of the road, the length of the dataset was cut to less than 30 seconds at higher speeds.

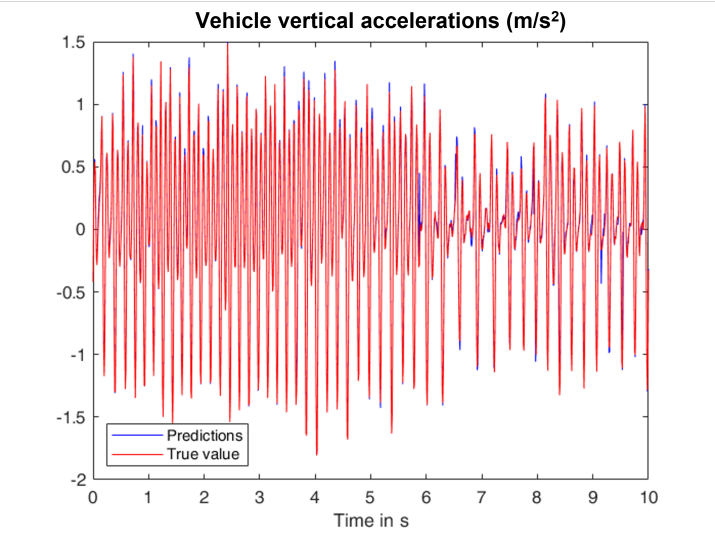


**(a)** Sprung mass acceleration when virtual sensor is trained with data of Z-axis only

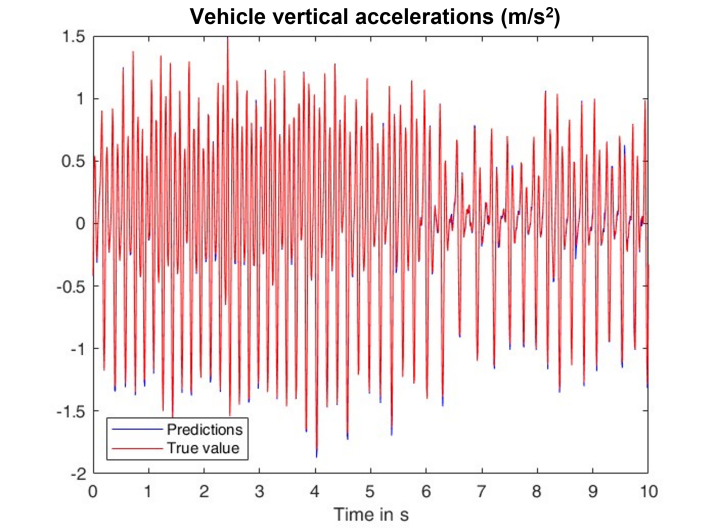


**(b)** Sprung mass acceleration when virtual sensor is trained with data of all 3 axes

**Figure 2.10:** Virtual sensor time-series performance for sinusoidal input considering different sprung mass acceleration axes for training the model

| Unsprung mass velocity front left | RMSE(m/s) | | $R^2$ | Mean absolute error(m/s) |
|---|---|---|---|---|
| | Validation | Testing | | |
| **Acceleration Z-only** | 0.0530 | 0.0658 | 0.9824 | 0.0393 |
| **Acceleration all axes** | 0.0501 | 0.0555 | 0.9870 | 0.0294 |

**Table 2.7:** Virtual sensor performance for sinusoidal input considering different axes of sprung mass acceleration for training the model

The performance of the virtual sensor is evaluated by first training it with acceleration along Z-axis followed by training it with all axes. The performance of the virtual sensor is reported in Table 2.7 and Figure 2.10.

There is not much of a difference in the performance of the virtual sensor between including only the Z-axis and including all axes. However, when considering the selected manoeuvres, it is possible to ignore the effect that the X and Y axes have on the outcome of the scenario. However, their effects

might need to be reexamined in light of the fact that there are a variety of potential manoeuvres and speeds at which the vehicle could be moving.

## 2.4. Discussion

The simulation results show that the virtual sensor that was made can accurately estimate the vertical speed of the unsprung mass in the situations that were looked at during both the testing and validation phases. This observation can be further substantiated by examining the plotted time series, which reveal a close resemblance between the estimated values and the actual unsprung mass velocity values.

Furthermore, the design decisions for the virtual sensor are justified through the evaluation of the developed model under various scenarios. Initially, the developed model is assessed across various forms of steering inputs. The model demonstrates comparable estimations between wheel steer angles and a combination of driver steering wheel angle and velocity. However, the latter option is preferred for the model due to the relative ease of measuring driver inputs compared to measuring wheel steer angles.

Subsequently, an assessment is conducted to examine the impact of roll, pitch, and yaw on the virtual sensor model that has been developed. The simulations demonstrate that the combination of pitch and roll yields better estimation performance. Lastly, the model is tested to see how it changes performance when different directions of sprung mass velocity are taken into account when training the model. The simulations show that the X and Y axes do not have much of an effect on how well the virtual sensor estimation works in the situations that were looked at.

# 3

# Suspension controller

This chapter will provide an explanation of the suspension control methods. Further, it will provide an overview of the control approach proposed against a standard reference which is used in this analysis.

Suspension control aims at maintaining/improving the required vehicle performance by controlling the suspension parameters. This control can be either model-based or data-driven. Model-based control methods include Skyhook, Groundhook, and hybrid strategies. Data-driven control methods include methodologies. Data-driven suspension control includes approaches such as fuzzy logic, artificial neural networks and modern approaches which use preview-based and learning-based methods.

In the examined controller models, there is distinction between model-based and data-driven control approaches. Even though a data-driven approach provides a good opportunity, the requirement of data for training the controller makes it dependent on model-based approaches. Since the principal requirement of the thesis is to reduce the vertical oscillations of the vehicle body, a skyhook controller is the best option. Skyhook control is easy to implement with information from a few sensors representing the vehicle state [15].

## 3.1. Skyhook control

The skyhook control strategy was developed primarily to improve the ride comfort performance of the vehicle. This is performed by minimizing the unsprung mass oscillations. In order to do that, the model introduces an imaginary damper that is connected to the sprung mass and a fixed point in the vertical space. The connection of the damper in such a way produces an additional force on the sprung mass negatively proportional to its velocity.

However, practically it is not possible to have a fixed point in space to have the skyhook damper connected. This is overcome by adding additional damping to emulate the imaginary force that would be generated by the Skyhook damper.

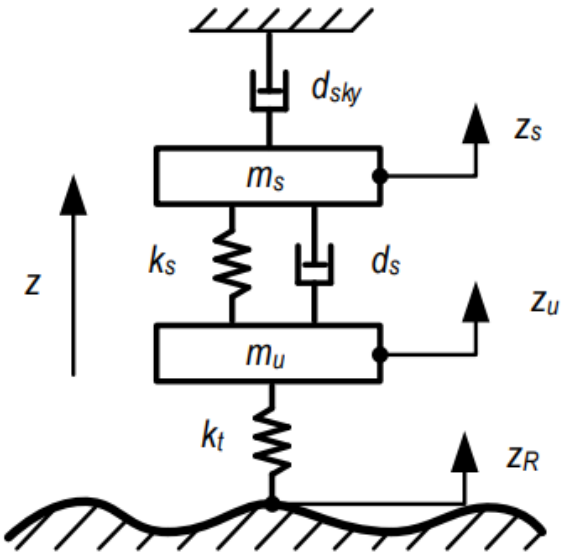


**Figure 3.1:** Skyhook model

Ideal system dynamics of skyhook control

$$m_s\ddot{z_s} = d_s(\dot{z_u} - \dot{z_s}) + k_s(z_u - z_s) - F_{sky} \tag{3.1}$$

$$m_u\ddot{z_u} = -d_s(\dot{z_u} - \dot{z_s}) - k_s(z_u - z_s) + k_t(z_R - z_u) \tag{3.2}$$

$$F_{sky} = d_{sky}\dot{z_s} \tag{3.3}$$

Various suspension control methods are used along with Skyhook control. Some of them include:

**2-State control** The 2-state control approach uses a switching damper that switches between a maximum and minimum damping ratio based on sprung and unsprung mass velocities.

$$d_s = \begin{cases} d_{max} & \text{if } \dot{z_s}(\dot{z_s} - \dot{z_u}) > 0 \\ d_{min} & \text{otherwise} \end{cases} \tag{3.4}$$

The benefit of this system is that its control output is extremely simply designed. Since the method only outputs the minimal or maximal damping ratio, the controller itself can be relatively simple. This has the benefit of being fast and responsive. It does not, however, approach the behaviour of an ideal Skyhook optimally.

**Linear control** The 2-state control can be improved by increasing the amount of control by adjusting the damping ratio of the variable damper. This way the system closely resembles the behaviour of the ideal Skyhook as the resulting force is now not only dependent on the suspension velocity but is also controlled by the varying damping ratio.

$$d_s = \begin{cases} sat\frac{\alpha_{sh}d_{max}(\dot{z_s} - \dot{z_u}) + (1-\alpha_{sh})d_{max}\dot{z_s}}{(\dot{z_s} - \dot{z_u})} & \text{if } \dot{z_s}(\dot{z_s} - \dot{z_u}) > 0 \\ d_{min} & \text{otherwise} \end{cases} \tag{3.5}$$

The parameter $\alpha_{sh}$ is the tuning parameter of the control model. It behaves like 2 state control when the tuning parameter is 1.

**Acceleration-driven damper control** This control technique uses acceleration of sprung masses instead of velocities in the 2-State control technique.

$$d_s = \begin{cases} d_{max} & \text{if } \ddot{z}_s(\ddot{z}_s - \ddot{z}_u) > 0 \\ d_{min} & \text{otherwise} \end{cases} \tag{3.6}$$

This form of control can be achieved with exactly the same sensors and actuation knowledge as the regular 2-state control. Usually, the signal of an accelerometer is used to determine the velocity by integration. In this case, the direct signal of the accelerometer can be used for the switching law. This alteration is therefore incredibly easy to implement for the Skyhook systems while it promises a significant improvement in comfort.

## 3.2. Control approach

The reference control approach employed in this study involves utilising a predetermined passive suspension system to determine the vehicle damping. Additionally, the estimation of sprung mass accelerations is achieved by subjecting the vehicle to different road profiles and velocities.

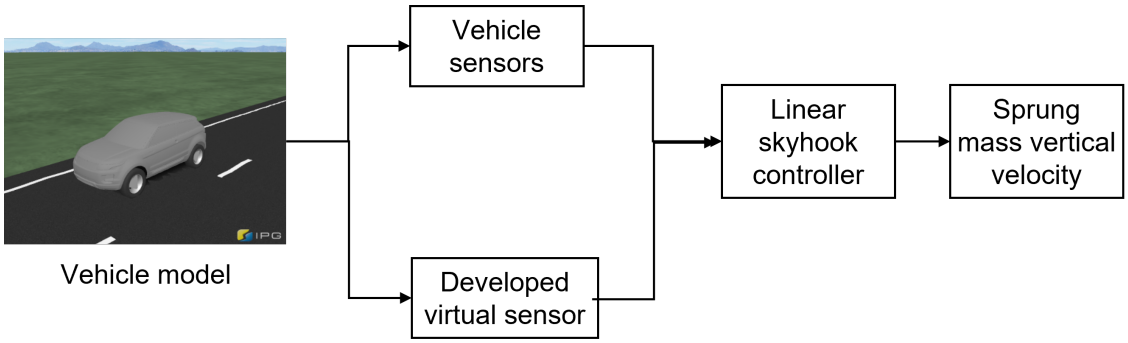


**Figure 3.2:** Proposed control approach

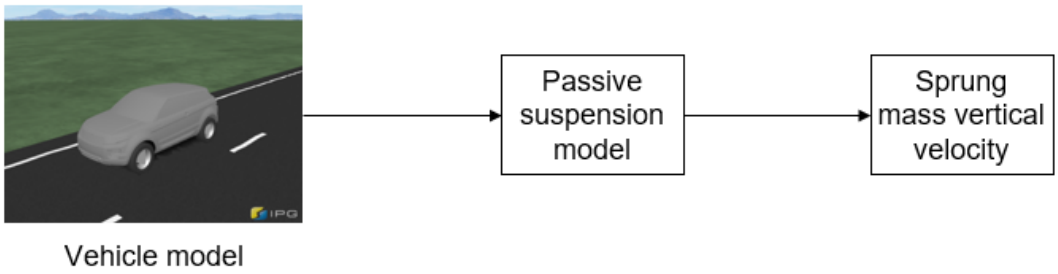


**Figure 3.3:** Reference control approach

The control system under consideration involves the utilisation of a linear skyhook controller, which is implemented within the Simulink software environment. The virtual sensor model that has been developed is exported to Simulink and subsequently integrated with the controller. The controller under consideration obtains input data from the IPG CarMaker software. The virtual sensor model incorporates various input parameters derived from real-time data obtained from the IPG CarMaker. These parameters encompass the steering angle and rate of the driver, the z-directional acceleration of the sprung mass, the roll angle and rate of the vehicle, the pitch angle and rate of the vehicle, and the angular velocity of each of the four wheels. The virtual sensor model subsequently computes and provides an estimate of unsprung mass velocity, which is subsequently inputted into the skyhook controller. Subsequently, the controller proceeds to assess the control force, which possesses the capability to

fluctuate within a pre-established range, and subsequently transmits this information back to the simulation.

The proposed controller is implemented in Simulink in accordance with Figure 3.2. The linear skyhook controller is developed individually for all four wheels and integrated with the corresponding unsprung mass vertical velocity sensors. The virtual sensor receives the vehicle data required from the IPG carmaker directly and estimates the unsprung mass vertical velocity. This estimation is then fed into the controller as an input to calculate the control force required as per Equation 3.5. The tuning parameters i.e. $\alpha_{sh}$ and the damping properties $d_{max}$ and $d_{min}$ are adjusted to achieve optimal suspension performance for each of the road conditions and velocities.

# 4

# Full vehicle simulation results

This section aims to present a thorough analysis and discussion of the simulation results derived from the comprehensive full vehicle simulations. Both simulation configurations will be subjected to testing, wherein each road profile will be employed in simulations conducted at different velocities. The road profiles encompass both parallel and angled corrugations, as well as cleat and fatigue surfaces. The velocities consist of three values: 10 km/h, 20 km/h, and 25 km/h. The scenario involves the car being driven in a straight line with constant speed and no steering or brake application. The evaluation time of the simulation is 20 seconds.

| Test name | Speeds in km/h | Evaluation time in seconds |
|---|---|---|
| **Parallel corrugations** | 10<br>20<br>25 | 20 |
| **Angled corrugations** | | |
| **Cleats** | | |
| **Fatigue** | | |

**Table 4.1:** Testing scenarios for ride comfort evaluation of the control systems

In order to assess the performance metrics related to ride comfort, measurements of vertical accelerations at the centre of gravity of the vehicle body will be obtained. The maximum values are also recorded and presented. Additionally, an analysis was conducted on the time series and frequency response of the vertical velocity of the output sprung mass.

## 4.1. Simulation results parallel corrugations

The initial series of simulations is conducted for the parallel corrugated road profile. The numerical simulations are presented in Table 4.2, which provides a comparison of the outcomes obtained from both the reference passive system and the proposed skyhook system. The time and frequency domain comparisons to the passive model are illustrated in Figure 4.1 and Figure 4.2 respectively.

| ***Parallel corrugations*** | **Reference system** | | | **Proposed system** | | | **% change in RMS $a_z$** |
|---|---|---|---|---|---|---|---|
| **Speed (km/h)** | **Min $a_z$ (m/s$^2$)** | **Max $a_z$ (m/s$^2$)** | **RMS $a_z$(m/s$^2$)** | **Min $a_z$ (m/s$^2$)** | **Max $a_z$ (m/s$^2$)** | **RMS $a_z$(m/s$^2$)** | |
| **10** | -4.647 | 3.965 | 1.509 | -4.218 | 3.619 | 1.424 | -5.632 |
| **20** | -5.575 | 6.986 | 1.637 | -3.971 | 4.476 | 1.366 | -16.534 |
| **25** | -5.558 | 5.690 | 1.395 | -4.872 | 5.250 | 1.216 | -12.866 |

**Table 4.2:** Comparison of reference and proposed system suspension performance in parallel corrugations.

The simulations demonstrate a significant improvement in performance across all velocities. The proposed system exhibits enhancements in both the root mean squared and peak values across all velocities. When comparing to the other velocities, the enhancement observed at a speed of 10 km/h exhibits a slightly lower magnitude.

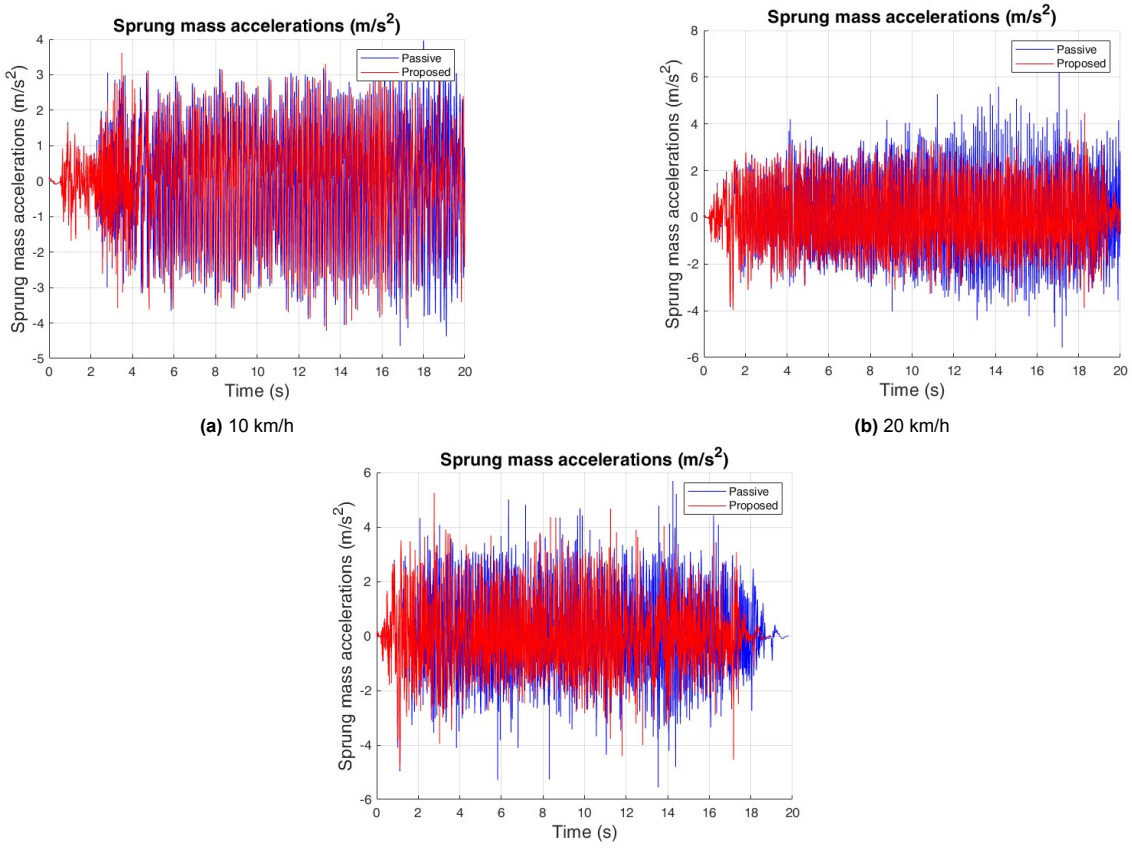


**(a)** 10 km/h

**(b)** 20 km/h

**(c)** 25 km/h

**Figure 4.1:** Time domain plot of sprung mass vertical accelerations at parallel corrugations

Similar inference can be drawn when observing the time-domain plots of the systems. The proposed system shows better control of sprung mass accelerations when compared to the reference system at all speeds. In the frequency domain, we can observe that the resonant peak values are lower in the proposed system at all velocities across the frequency spectrum.

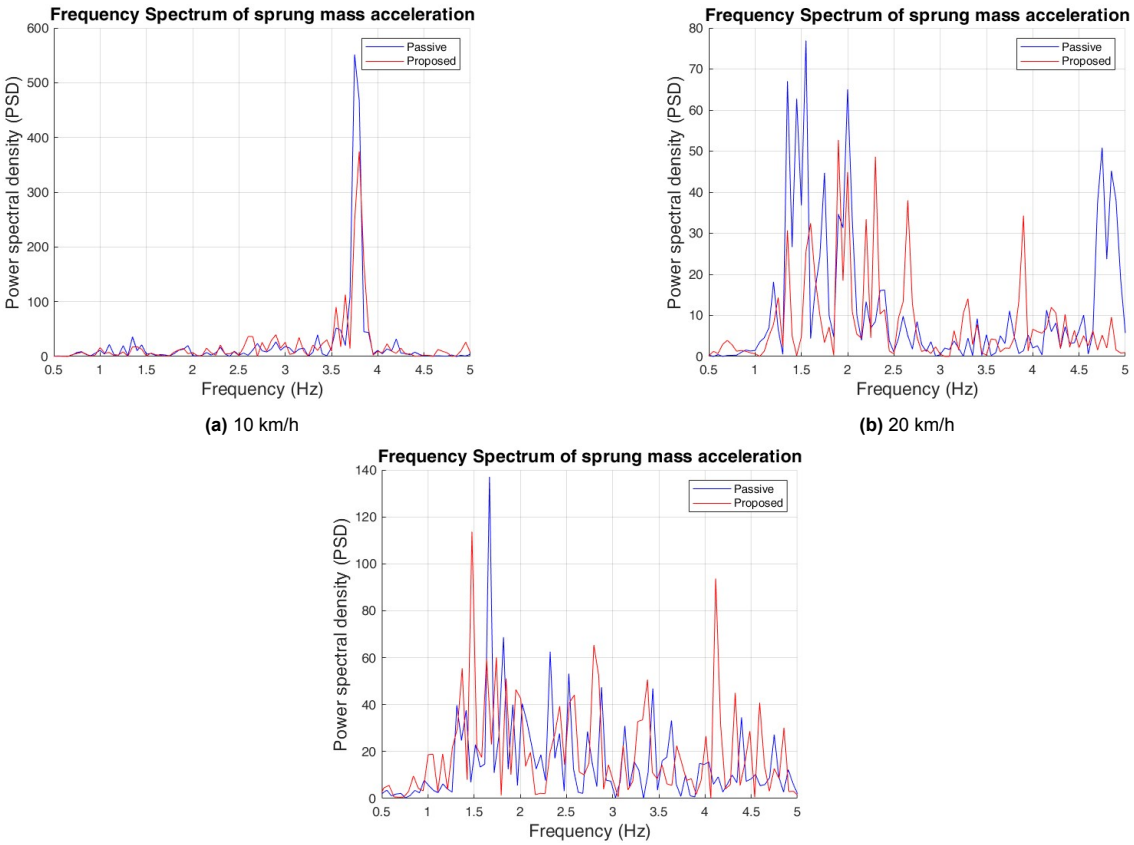


**(a)** 10 km/h

**(b)** 20 km/h

**(c)** 25 km/h

**Figure 4.2:** Frequency response plot of sprung mass vertical accelerations at parallel corrugations

## 4.2. Simulation results angled corrugations

The next series of simulations is conducted for the angled corrugated road profile. The numerical simulations are presented in Table 4.3, which provides a comparison of the outcomes obtained from both the reference passive system and the proposed skyhook system. The time and frequency domain comparisons to the passive model are illustrated in Figure 4.3 and Figure 4.4 respectively.

| ***Angled corrugations*** | **Reference system** | | | **Proposed system** | | | **% change in RMS $a_z$** |
|---|---|---|---|---|---|---|---|
| **Speed (km/h)** | **Min $a_z$ ($m/s^2$)** | **Max $a_z$ ($m/s^2$)** | **RMS $a_z$($m/s^2$)** | **Min $a_z$ ($m/s^2$)** | **Max $a_z$ ($m/s^2$)** | **RMS $a_z$($m/s^2$)** | |
| **10** | -4.169 | 3.607 | 1.136 | -3.886 | 3.494 | 1.110 | -2.306 |
| **20** | -6.168 | 5.578 | 1.587 | -5.081 | 5.608 | 1.195 | -24.702 |
| **25** | -5.956 | 5.655 | 1.217 | -5.186 | 5.787 | 1.130 | -7.149 |

**Table 4.3:** Comparison of reference and proposed system suspension performance in angled corrugations.

The simulations demonstrate a significant enhancement in performance across all velocities. The proposed system exhibits enhancements in both the root mean squared and peak values in almost across all velocities. When comparing to the other velocities, the enhancement observed at a speed of 10 km/h exhibits a slightly lower magnitude. The peak value in the positive side of the proposed system at 20 km/h and 25 km/h does not show improvement when compared to the reference system.

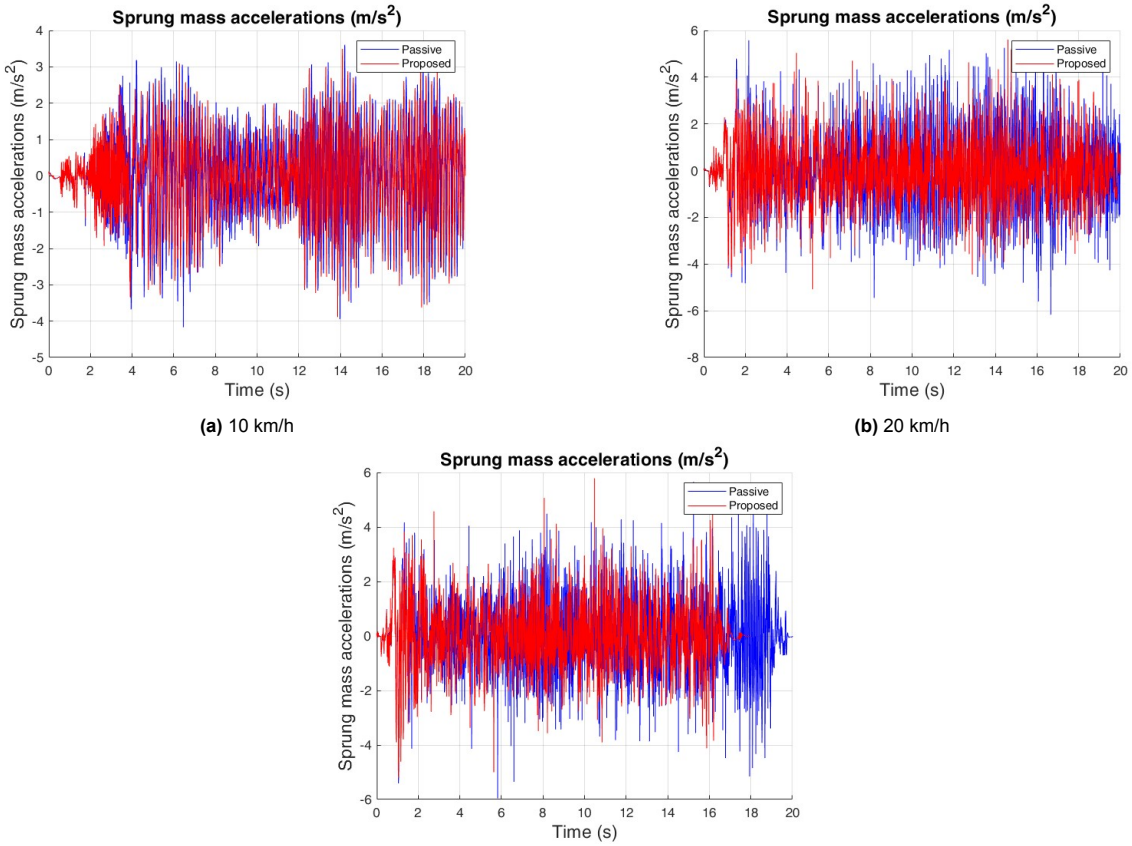


**(a)** 10 km/h

**(b)** 20 km/h

**(c)** 25 km/h

**Figure 4.3:** Time domain plot of sprung mass vertical accelerations at angled corrugations

The proposed system shows slightly better control of sprung mass accelerations when compared to the reference system at all speeds. In the frequency domain, we can observe that the peak values are lower in the proposed system at velocities 10 km/h and 20 km/h across the frequency spectrum. At 25 km/h, at lower frequencies, the proposed system show better control, however at above 3.5 Hz, the proposed system performance deteriorates. Nevertheless, these frequencies do not hold substantial significance when it comes to evaluating ride comfort.

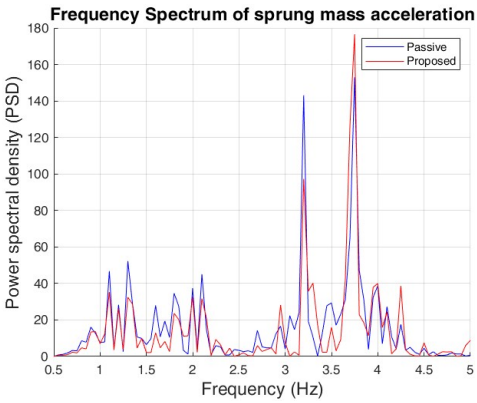


**(a)** 10 km/h

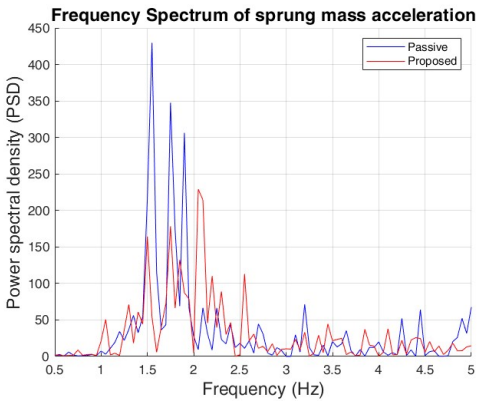


**(b)** 20 km/h

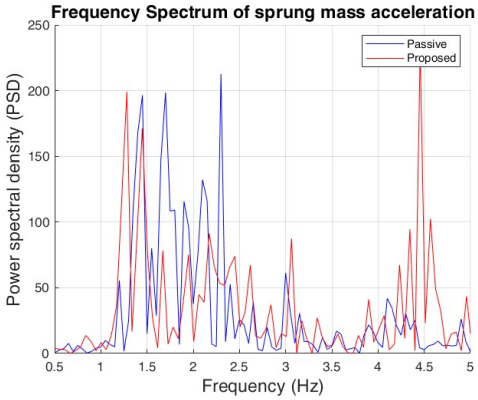


**(c)** 25 km/h

**Figure 4.4:** Frequency response plot of sprung mass vertical accelerations at angled corrugations

## 4.3. Simulation results cleats

The next series of simulations is conducted for the cleats road profile. The numerical simulations are presented in Table 4.4, which provides a comparison of the outcomes obtained from both the reference passive system and the proposed skyhook system. The time and frequency domain comparisons to the passive model are illustrated in Figure 4.5 and Figure 4.6 respectively.

| ***Cleats*** | **Reference system** | | | **Proposed system** | | | **% change in RMS $a_z$** |
|---|---|---|---|---|---|---|---|
| **Speed (km/h)** | **Min $a_z$ ($m/s^2$)** | **Max $a_z$ ($m/s^2$)** | **RMS $a_z$($m/s^2$)** | **Min $a_z$ ($m/s^2$)** | **Max $a_z$ ($m/s^2$)** | **RMS $a_z$($m/s^2$)** | |
| **10** | -3.974 | 7.018 | 1.155 | -3.867 | 4.797 | 1.070 | -7.335 |
| **20** | -7.071 | 10.219 | 1.725 | -7.508 | 9.857 | 1.573 | -8.797 |
| **25** | -6.243 | 6.557 | 1.497 | -5.709 | 6.317 | 1.447 | -3.359 |

**Table 4.4:** Comparison of reference and proposed system suspension performance in cleats.

The simulations demonstrate a significant enhancement in performance across all velocities. The proposed system exhibits enhancements in both the root mean squared and peak values in almost across all velocities. When comparing to the other velocities, the enhancement observed at a speed of 25 km/h exhibits a slightly lower magnitude.

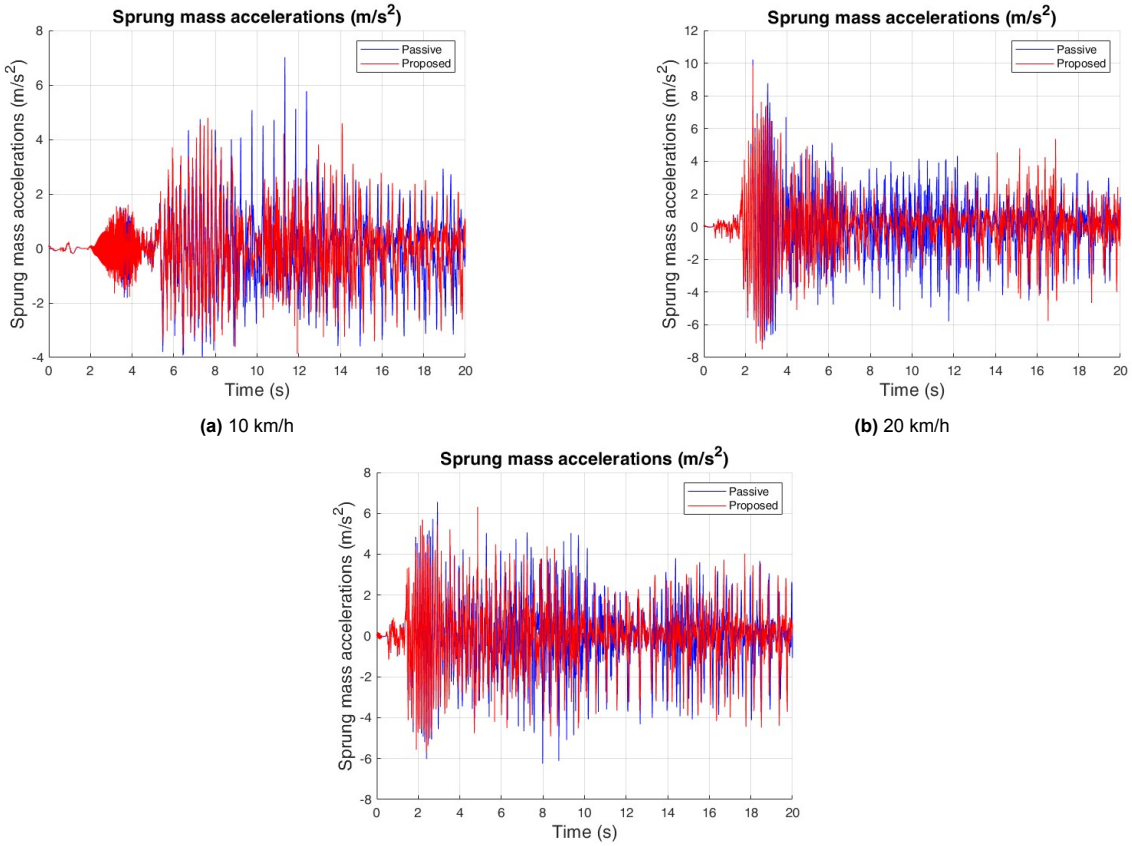


**(a)** 10 km/h

**(b)** 20 km/h

**(c)** 25 km/h

**Figure 4.5:** Time domain plot of sprung mass vertical accelerations at cleats

The proposed system shows slightly better control of sprung mass accelerations when compared to the reference system at all speeds. In the frequency domain, we can observe that the peak values are lower in the proposed system at 10 km/h . At 20 km/h and 25 km/h, at lower frequencies, the proposed system show better control, however at higher frequencies, the proposed system performance deteriorates. Nevertheless, these frequencies do not hold substantial significance when it comes to evaluating ride comfort.

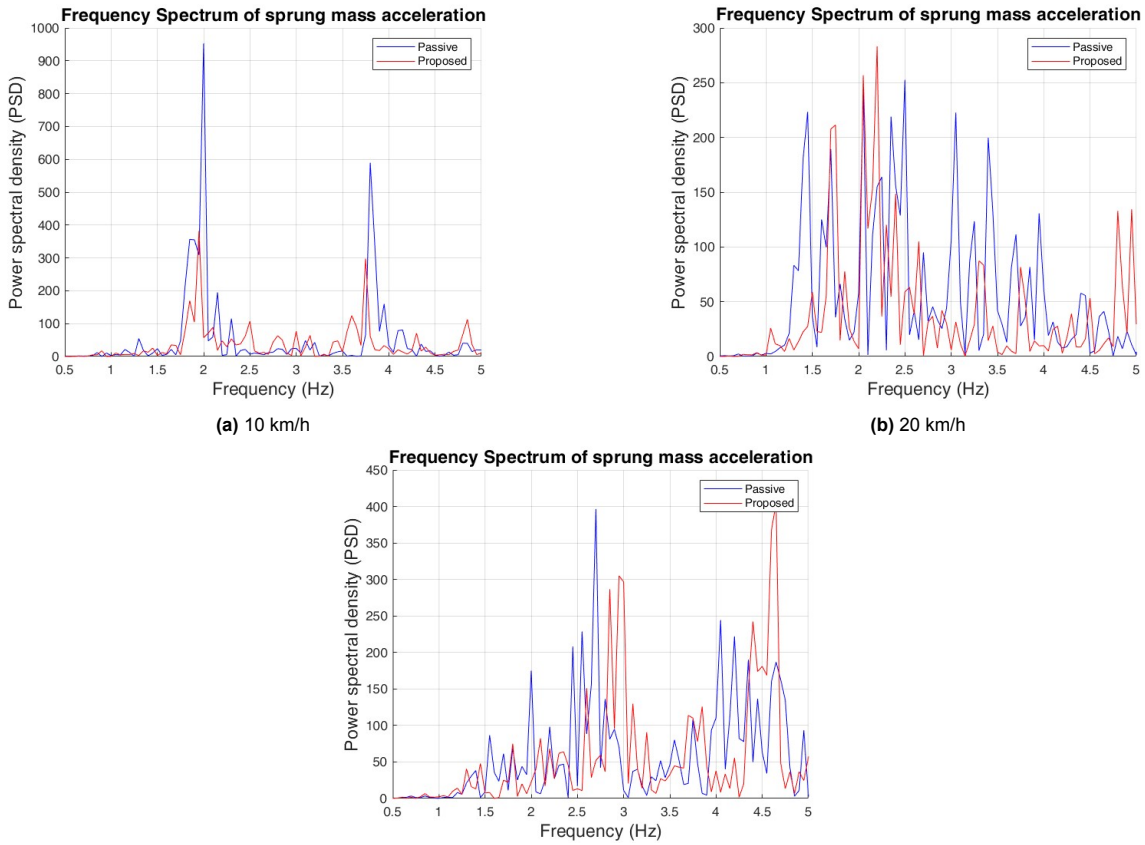


**(a)** 10 km/h

**(b)** 20 km/h

**(c)** 25 km/h

**Figure 4.6:** Frequency response plot of sprung mass vertical accelerations at cleats

## 4.4. Simulation results fatigue surface

The final series of simulations is conducted for the fatigue surface. The numerical simulations are presented in Table 4.5, which provides a comparison of the outcomes obtained from both the reference passive system and the proposed skyhook system. The time and frequency domain comparisons to the passive model are illustrated in Figure 4.7 and Figure 4.8 respectively.

| ***Fatigue surface*** | **Reference system** | | | **Proposed system** | | | **% change in RMS $a_z$** |
|---|---|---|---|---|---|---|---|
| **Speed (km/h)** | **Min $a_z$ (m/s$^2$)** | **Max $a_z$ (m/s$^2$)** | **RMS $a_z$(m/s$^2$)** | **Min $a_z$ (m/s$^2$)** | **Max $a_z$ (m/s$^2$)** | **RMS $a_z$(m/s$^2$)** | |
| **10** | -4.211 | 4.322 | 0.980 | -3.894 | 4.083 | 0.893 | -8.878 |
| **20** | -5.233 | 5.825 | 1.732 | -4.717 | 5.147 | 1.583 | -8.615 |
| **25** | -5.311 | 6.019 | 1.694 | -5.146 | 6.333 | 1.566 | -7.528 |

**Table 4.5:** Comparison of reference and proposed system suspension performance in fatigue surface.

The simulations demonstrate a significant enhancement in performance across all velocities. The proposed system exhibits enhancements in both the root mean squared and peak values in almost across all velocities. The peak value in the positive side of the proposed system at 25 km/h show slightly higher values when compared to the reference system.

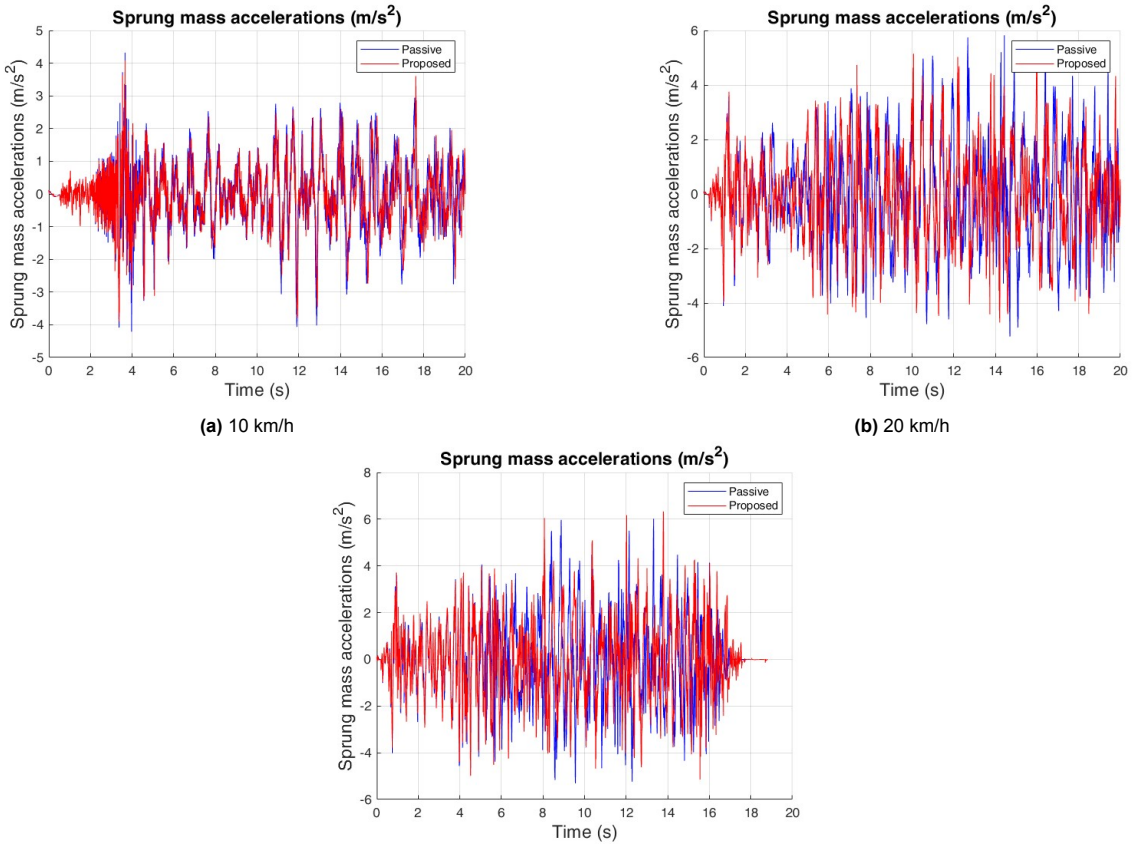


**(a)** 10 km/h

**(b)** 20 km/h

**(c)** 25 km/h

**Figure 4.7:** Time domain plot of sprung mass vertical accelerations at fatigue surface

The proposed system shows slightly better control of sprung mass accelerations when compared to the reference system at all speeds. In the frequency domain, we can observe that the peak values are lower in the proposed system at all velocities across the frequency spectrum.

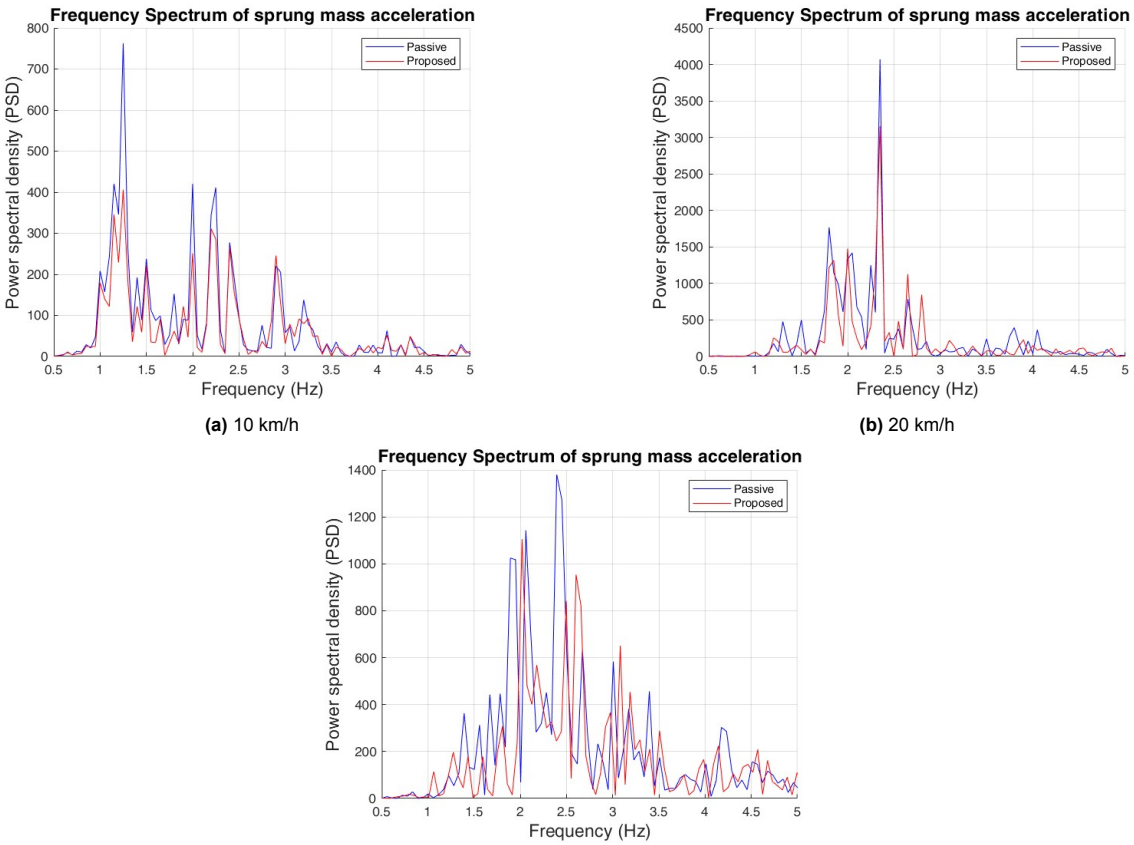


**(a)** 10 km/h

**(b)** 20 km/h

**(c)** 25 km/h

**Figure 4.8:** Frequency response plot of sprung mass vertical accelerations at fatigue surface

## 4.5. Discussion

The study examined the effects of utilising neural network-based data-driven virtual sensors on the comfort metric root mean square (RMS) of vertical acceleration of the sprung mass. Specifically, the analysis focused on the implementation of these virtual sensors in conjunction with a linear Skyhook control algorithm. The resulting measurements were then compared to data obtained from a passive suspension model. In addition to assessing the metrics, the analysis also includes an evaluation of the time series and frequency response of the vertical accelerations of the sprung mass.

The developed virtual sensor shows improvement in the sprung mass acceleration metric at the scenarios considered. The scenarios include various extreme road surfaces such as angled and parallel corrugations, cleats and fatigue surfaces along with three different speeds (10 km/h, 20 km/h and 25 km/h). No investigation is done at higher speeds as safe driving cannot be ensured by moving faster in the selected scenarios.The virtual sensor developed in this study demonstrates improvements in both the peak-to-peak magnitude values and the resonant peaks observed in the frequency domain.

# 5
# Conclusions

The goal of this research is the evaluation of ride comfort by data-driven virtual sensing of unsprung mass vertical velocity. A neural network based virtual sensor is developed for this purpose to estimate the unsprung mass vertical velocity. The virtual sensor is then evaluated for its estimation performance and its robustness to different input parameters. This model is then integrated with a linear skyhook suspension controller. The proposed controller is then assessed in comparison to a reference passive suspension system for ride comfort performance. The evaluation is conducted under different velocities and types of road conditions. In this final chapter, the conclusions and recommendations are presented.

## 5.1. Conclusions

- The vertical velocity estimator for the unsprung mass that has been developed demonstrates a high level of accuracy in estimating values for the specific scenarios being examined. The average RMS error of estimation of unsprung mass velocity was around 0.075 m/s while the coefficient of determination($R^2$) was around 0.98.

- The unsprung mass vertical velocity estimator that has been developed demonstrates robustness to the chosen input parameters during its development for the examined scenarios.

- The comprehensive vehicle simulations conducted on the proposed system demonstrate enhancements in both the root mean square (RMS) and peak values of the accelerations experienced by the sprung mass across nearly all the analysed scenarios. The reduction in RMS values is approximately 11 percent in parallel and angled corrugations, whereas in cleats and fatigue surface, the improvement is approximately 7 percent. The degree of improvement is contingent upon the longitudinal velocity of the vehicle.

- The time series of the proposed system also echoes the improvement seen in the metrics. Further, the frequency response of the sprung mass accelerations also show a decrease in peak values for the proposed system.

## 5.2. Recommendations

The proposed method has further potential to improve the ride comfort performance of an automobile. Further research is necessary in order to more comprehensively understand the potential of the virtual sensing approach. The following are the recommendations to further advance this research:

- The unsprung mass velocity estimator can be enhanced by incorporating additional scenarios, thereby increasing its robustness. At present, it is assumed that the vehicle is driven in a straight line at a constant velocity, and the incorporation of vehicle steering, braking and acceleration is not taken into account in the development of the model.

- The virtual sensor estimator currently considers extreme road surfaces and lower speeds for its development. Incorporation of additional surfaces and higher speeds will make the model more robust and more realistic.

- The controller currently uses a linear skyhook controller and assumes that the suspension damping properties can be altered with different velocities. Additional control methods such as sliding mode control, model predictive control etc. should be investigated along with the developed virtual sensor for its effect on ride comfort performance.

- Studies show that ride comfort cannot be completely described by objective metrics [16]. Subjective assessments should be carried out for the proposed methodology to further assess the practical impact of the developed method.

# Bibliography


[1] Guido Koch. “Adaptive control of mechatronic vehicle suspension systems”. PhD thesis. Technische Universität München, 2011.

[2] Johan Theunissen et al. “Preview-based techniques for vehicle suspension control: a state-of-the-art review”. In: *Annual Reviews in Control* 51 (June 2021). DOI: 10.1016/j.arcontrol.2021.03.010.

[3] AMA Soliman and MMS Kaldas. “Semi-active suspension systems from research to mass-market – A review”. In: *Journal of Low Frequency Noise, Vibration and Active Control* 40 (Oct. 2019), p. 146134841987639. DOI: 10.1177/1461348419876392.

[4] Mostafa Ghoniem, Taher Awad, and Ossama Mokhiamar. “Control of a new low-cost semi-active vehicle suspension system using artificial neural networks”. In: *Alexandria Engineering Journal* 59 (July 2020). DOI: 10.1016/j.aej.2020.07.007.

[5] Sathishkumar P et al. “Energy harvesting approach to utilize the dissipated energy during hydraulic active suspension operation with comfort oriented control scheme”. In: *Energy* 224 (Feb. 2021), p. 120124. DOI: 10.1016/j.energy.2021.120124.

[6] Sean Campbell et al. “Sensor Technology in Autonomous Vehicles : A review”. In: *2018 29th Irish Signals and Systems Conference (ISSC)*. 2018, pp. 1–4. DOI: 10.1109/ISSC.2018.8585340.

[7] Haorong Li, Daihong Yu, and James Braun. “A review of virtual sensing technology and application in building systems”. In: *HVAC&R Research* 17 (Oct. 2011), pp. 619–645. DOI: 10.1080/10789669.2011.573051.

[8] Claudio Giovanni Mattera et al. “A Method for Fault Detection and Diagnostics in Ventilation Units Using Virtual Sensors”. In: *Sensors* 18.11 (2018). ISSN: 1424-8220. DOI: 10.3390/s18113931. URL: https://www.mdpi.com/1424-8220/18/11/3931.

[9] Catalin Victor Zaharia and Adrian Clenci. “Study on virtual sensors and their automotive application”. In: (Jan. 2013).

[10] Shan-Bin Sun et al. “A Data-Driven Response Virtual Sensor Technique with Partial Vibration Measurements Using Convolutional Neural Network”. In: *Sensors* 17.12 (2017). ISSN: 1424-8220. DOI: 10.3390/s17122888. URL: https://www.mdpi.com/1424-8220/17/12/2888.

[11] Nils Pletschen and Patrick Badur. “Nonlinear State Estimation in Suspension Control Based on Takagi-Sugeno Model”. In: *IFAC Proceedings Volumes* 47 (2014), pp. 11231–11237.

[12] Marco Viehweger et al. “Vehicle state and tyre force estimation: demonstrations and guidelines”. In: *Vehicle System Dynamics* 59 (Jan. 2020), pp. 1–28. DOI: 10.1080/00423114.2020.1714672.

[13] Eldar Šabanovič et al. “Feasibility of a Neural Network-Based Virtual Sensor for Vehicle Unsprung Mass Relative Velocity Estimation”. In: *Sensors* 21.21 (2021). ISSN: 1424-8220. DOI: 10.3390/s21217139. URL: https://www.mdpi.com/1424-8220/21/21/7139.

[14] Paulius Kojis, Eldar Šabanovič, and Viktor Skrickij. “Deep neural network based data-driven virtual sensor in vehicle semi-active suspension real-time control”. In: *Transport* 37 (June 2022), pp. 37–50. DOI: 10.3846/transport.2022.16919.

[15] Changning Liu et al. “General Theory of Skyhook Control and Its Application to Semi-active Suspension Control Strategy Design”. In: *IEEE Access* PP (July 2019), pp. 1–1. DOI: 10.1109/ACCESS.2019.2930567.

[16] Schalk Els. “The applicability of ride comfort standards to off-road vehicles”. In: *Journal of Terramechanics* 42 (Jan. 2005), pp. 47–64. DOI: 10.1016/j.jterra.2004.08.001.